AD-A139 199 A STUDY OF SLENDER THIN CONICALLY CAMBERED WINGS WITH FLOW SEPARATION REV..(U) BRISTOL UNIV (ENGLAND) DEPT OF AERONAUTICAL ENGINEERING R K NANGIA JUN 80 RKN/7701 1/1

UNCLASSIFIED AFOSR-77-3243 F/G 20/4 NL

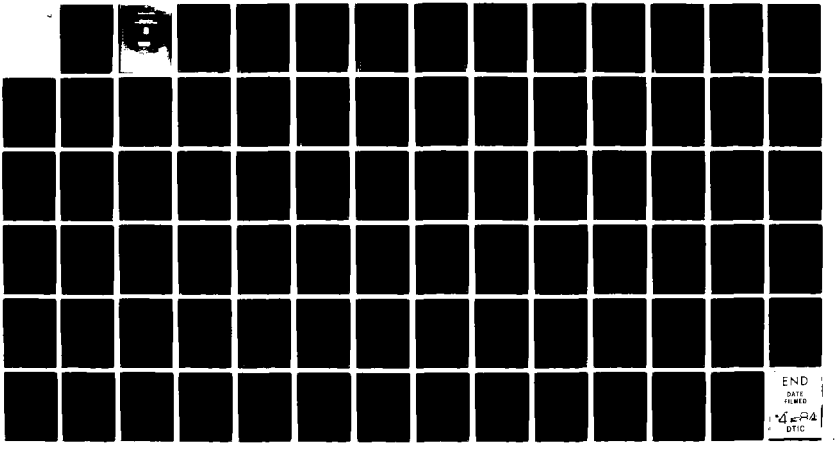

END
DATE FILMED
DTIC

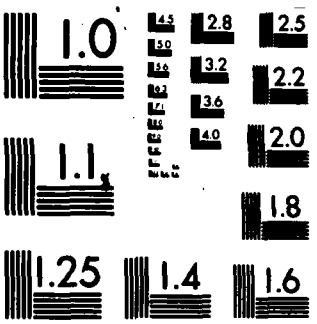

MICROCOPY RESOLUTION TEST CHART
NATIONAL BUREAU OF STANDARDS-1963-A

GRANT NUMBER US AFOSR-77-3243

A STUDY OF SLENDER, THIN CONICALLY CAMBERED WINGS WITH FLOW SEPARATION.

R. K. Nangia

Department of Aeronautical Engineering,

University of Bristol, U.K.

October 1977

Revised June 1980

Part of

Final Report 1st February, 1977 - 30th April, 1979.

Prepared for:

Air Force Flight Dynamics Laboratory/FXM
Wright-Patterson AFB, Ohio 45433, U.S.A.

and

European Office of Aerospace Research and Development,
London, U.K.

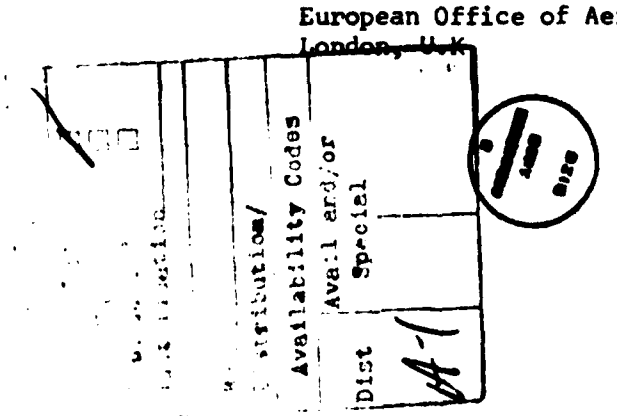

REPORT DOCUMENTATION PAGE		READ INSTRUCTIONS BEFORE COMPLETING FORM
1. Report Number	2. Govt Accession No. AD-A139199	3. Recipient's Catalog Number
4. Title (and Subtitle) A STUDY OF SLENDER, THIN CONICALLY CAMBERED WINGS WITH FLOW SEPARATION		5. Type of Report & Period Covered Part of Final Report (Feb. 1977 to April 1979) 6. Performing Org. Report Number Dept of Aeronautical Engineering University of Bristol, RKN/7701
7. Author(s) R. K. NANGIA		8. Contract or Grant Number AFOSR-77-3243
9. Performing Organization Name and Address Department of Aeronautical Engineering, University of Bristol, Queen's Building, University Walk, Bristol, BS8 1TR, England.		10. Program Element, Project, Task Area & Work Unit Numbers PE - 61102F Proj - 2301 Task - D1
11. Controlling Office Name and Address Air Force Flight Dynamics Laboratory/FXM Wright-Patterson AFB, OH 45433		12. Report Date October 1977 (Revised ~~July~~ Jan 1980) 13. Number of Pages
14. Monitoring Agency Name and Address EOARD/LNV, Box 14, FPO New York 09510		15.

16. & 17. Distribution Statement

Approved for public release; distribution unlimited.

18. Supplementary Notes

Revised July 1980

19. Key Words

Slender Wings, Conical Wings, Cambered Wings, Leading edge droop, Vortices, Flow separation.

20. Abstract Efficient wing design for high speed flight, good transonic manoeuverability and satisfactory near-to-ground performance requires detailed understanding of flow around leading edges with and without separations.

Slender body theory with exact boundary condition has been used to calculate flow past thin conically cambered wings. The flow separations have been modelled as vortex-cut arrangements.

Leading edge camber has a very marked effect on wing pressures, hence on the overall aerodynamic force. The lift drag ratio can be enhanced by leading edge droop.

An interesting feature is the indication of multiple-valued solution for realistic cambers, and points to existence of more than one pair of vortex separation systems.

The method may be extended to include thickness effects, secondary vortices, vortex sheet separations, planform effects, leading edge devices or extensions.

FORM 1473

CONTENTS

SUMMARY

There is considerable interest in the subject of efficient wing design for high speed flight, together with good manoeuverability at transonic speed and satisfactory near-to-the-ground performance. An important area is the detail design of wing leading edges with or without leading devices and variable camber, the flow may be attached or separated.

In this report, slender body theory with exact boundary condition is used to calculate the flow past a thin conically cambered wing (i.e. with drooped leading edges). The leading edge flow separation has been modelled as a vortex-cut arrangement.

Calculated results suggest that the leading edge camber has a very marked effect on the local pressures near the leading edges, and hence on the overall aerodynamic forces. In particular, the lift-drag ratio can be enhanced by suitable choice of leading edge droop.

An interesting feature of the results is the indication of multiple-valued solution for realistic cambers, i.e. when the shoulder of the droops is very near the leading edge. In experiment this is not likely and another separation system may exist near the high curvature wing section. The work in

this report therefore points to inadequacy of current design approaches with simulation of one vortex system only.

The method of this report may also be extended to incorporate, thin extensions of wing span, leading edge devices, secondary vortices and variation of separation points. Cross-section thickness may also be included. More complex vortex sheet representation of the separation may also be incorporated. From the point of view of aircraft manoeuverability, wing root gaps or leading edge gaps are of interest. Another consideration is for the asymmetrical effects.

LIST OF SYMBOLS

a	OA in Z-plane, Fig.5.
a_1	radius of circle in Z_o-plane, Fig.5.
A	aspect ratio = 4k.
B'	defined by equation (33).
C	defined by equation (32).
c	CB in Z-plane, Fig.5.
$\bar{c}$	c/a
C_L	lift coefficient.
$C_{L_{lin}}$	linear lift coefficient.
$C_{L_{nlin}}$	non-linear lift coefficient.
C_D	drag coefficient.
C_{D_i}	lift induced drag coefficient.
C_{D_p}	profile drag.
e_1, f_1	defined by $Z\, e^{3i\phi} = e_1 + i\, f_1$
f	function
$g(\psi)$	defined in Appendix A.
G	defined in Appendix A.
h	given by $h^2 = 1 + (1/\bar{c}^2)$
H	defined in Fig.4. - amount of leading edge droop
$\mathcal{I}$	imaginary part
I_1	defined by equation (40)
J_A	defined in Appendix A.
J_B	defined in Appendix A.
k	cot (angle of sweep)
k_1	lift dependent drag factor $\pi A C_D/C_L^2$
L	lift

M,N	defined in section II.7
n	defined in Fig.4.
$\mathcal{R}$	real part.
R	radius of circle in Z_3-plane in Fig.5 (= a/sinδcosδ).
r	OP in Z_1-plane, Fig.5.
$\underline{r}$	CP' in Z_1-plane, Fig.5.
r'	parameter in equation (10)
s	semi-span
T	vertical slit plane, Fig.5. $T = y_T + iz_T$
T_e	vertical slit plane, Fig.5. $T_e = y_{T_e} + iz_{T_e}$
T_{e_1}	vortex position in T_e-plane, Fig.5.
u,v,w	perturbation velocities in x,y,z system.
V	velocity at infinity.
v_n	velocity component normal to surface in cross-flow plane.
W	complex velocity potential.
W_j	(j = 1,2,3,4) defined in section II.4.
x,y,z	Cartesian coordinates.
Z	y + iz
Z_v	$y_v + iz_v$ vortex position in Z-plane.
Z_j	$y_j + i\,z_j$ (j = 0,1,2,3) complex planes see Fig.5.
α	angle of incidence.
α_o	angle of incidence at zero lift.
α_D	defined in equation (39)
α_s	angle of incidence for no singularity at the leading edge.
β	tanδ
δ	half the angle AO'B in Z_2-plane, Fig.5.
Γ	vortex strength.
ε	droop angle as defined in Fig.4.
ε_1	defined in section II.6.

θ angle POA in Z_1-plane, Fig.5.

κ lift dependent drag factor = $\pi AC_D/C_L^2$.

λ angle $PO'y_o$ in Z_o-plane, Fig.5.

ρ density.

ϕ half angle POB in Z_2-plane, Fig.5.

Φ velocity potential.

$\frac{\partial \Phi}{\partial n}$ normal component of velocity in cross-flow plane.

ψ defined by $\sin\psi = \tan\phi/\tan\delta$

suffix u refers to the upper surface.

ℓ refers to the lower surface.

superscript ' refers to variable quantity in integration.

subscript L or L.E. refers to leading edge

v refers to vortex

I INTRODUCTION

There is considerable interest in the subject of efficient wing design for high speed flight together with good manoeuverability at transonic speed and satisfactory near-to-ground performance. An important area is the detail design of wing leading edges with or without leading edge devices and variable camber. The flow may be attached or separated.

The designer is faced with simultaneous constraints of efficient high-speed cruise (at low lift coefficient C_L, high Mach number M), satisfactory take-off and landing performance (at high C_L, low M) and good transonic manoeuverability (low to high C_L, M near 1). These constraints necessarily result in performance limiting compromises. By way of an example, we take the case of an aircraft with highly swept-back wings (Figure 1a) or having a portion which is highly swept-back (Figure 1b). It has been shown that gains in flying efficiency i.e. lift-drag ratio, can be obtained by drooping the leading edge. The amount of droop and its geometry, e.g. the shoulder position depends on the operating C_L. Thus for low C_L values the optimum position of the shoulder of the droops may be near the leading edge, whilst at higher values of C_L, better results are obtained with somewhat gentler camber shapes (Figure 1c). The choice of droop is subject to compromises of this nature.

The extent of such limiting compromises can be reduced by permitting the designer with greater flexibility in the geometric configuration. One approach is the use of fixed or variable geometry near the leading edges. Variable camber with or without slats or other devices (Figure 1d) fall into this category.

For conventional aircraft with wings of low sweep-b[illegible] there is a considerable amount of information available [illegible] the subject of leading edge design with or without devices (R[illegible]1). Calculation methods have been devised for treating 2-D geometries (Figs. 2 and 3). The methods are strictly applicable only when 3-D effects such as those due to wing-tips or fuselage junctions, are small.

For wings of higher sweep-back, however, there seems to be only a small amount of information available, particularly with regard to leading edge devices. An idea of the order of gains from leading edge devices can be obtained by reference to the work of Ray and Hollingsworth (Ref.2) on F-4 Fighter aircraft with leading edge sweep-back 51.4°. They conclude that incorporation of devices resulted in a sizable 33% improvement on the buffet onset, L/D performance gain of 35% at C_L = .8 and improved lateral directional characteristics throughout the test Mach number range of 0.6 to 0.94. The improvements were verified in a subsequent flight evaluation.

Goodmanson and Gratzer (Ref.3) show 24% improvement in L/D at C_L = 0.4, using droop and slats on a highly sweep-back wing.

At present there are no suitable methods which take into account the flow separation and are generally applicable. There are, however, a few attempts to solve the 3-D wings with separation under development. These are of panel or collocation type. They require a great deal of computer time and use large cores in the computer. It is not clear whether these methods will permit adequate resolution with panels or collocation points to deal with high curvature droops near the leading edges, or leading edge devices, or secondary vortices.

There have been however a number of attempts (Refs. 4 to 16) to calculate the flowfields within the framework of slender body theory. The slender body theory is applicable in subsonic or moderately supersonic flow (i.e. the component of flow normal to the wing leading edge is less Mach 0.6). Refs. 4 - 7 concentrate on attached flow. In particular, Cooke (Ref.7) deals with very general and realistic droop configurations. The flows calculated are however for the particular case where the leading edge singularity vanishes. Refs. 8-12 idealise the flow separations by line vortex-cut arrangements. Attempt has been made only to calculate the flows for flat or circular arc camber wings. The approach of Jobe(10) although nominally for general camber ignores the zero incidence flows.

In Refs. 13-16, the leading edge separations are more realistically modelled by vortex sheet representations. Once again only the uncambered wing and circular arc camber cases have been fully considered. A more general approach by

Fernandez and Holla (16) does not include the camber effects at zero incidence directly. In this report an attempt has been made to calculate the flows around general wing camber shapes with droop on basis of Ref.7 and idealised vortex-cut arrangements as in Ref.8. This procedure is considered to be an essential step before embarking on more complicated vortex sheet representation.

It must be mentioned that the attached flow solutions can be obtained by not including the separation effects.

The method of this report may also be extended to incorporate, thin extensions of wing span, leading edge devices, secondary vortices and variation of separation points. Cross-section thickness may also be included.

II THEORETICAL FORMULATION

II.1 Equation of Motion

Equation of motion to be satisfied is the well known Laplace Equation which represents a slightly perturbed main stream velocity V and corresponding Mach Number M:

$$(1 - M^2)\Phi_{xx} + \Phi_{yy} + \Phi_{zz} = 0.$$

where Φ is the disturbance velocity potential and x, y, z are Cartesian co-ordinates fixed to the wing (x-axis along the centre line of the wing Fig.4).

The flow-field is restricted to highly swept wings and the term $(1 - M^2)\Phi_{xx}$ may be neglected. The equation of motion then becomes Laplace's equation in y and z dimensions

$$\Phi_{yy} + \Phi_{zz} = 0.$$

This is the governing equation of motion of slender wing (or body) theory and applies throughout the Mach number range.

II.2 Boundary Conditions and Flow Model

The conditions on the wing are:

(i) The wing is solid and hence the normal velocities are zero.

(ii) For attached flow at the leading edge the condition is that the flow turns around the leading edge. If the edge is sharp the velocity is infinite.

If the flow separates at the leading edge, the condition to be applied is that the velocity is finite at the edge.

The conditions in the field are:

(i) The disturbances vanish at infinity.

(ii) The fluid Pressure is continuous.

A conical wing with leading edge drooped, at incidence α to the freestream V and with Cartesian axes xyz is shown in Fig.1. The semi-span of the wing is $s=kx$ and the shoulder is distance ns from the centre, the amount of droop is Hs.

The model approximates the vorticity in the separated vortex sheets from the leading edge $(\pm s(x), -Hs)$ by a concentrated pair of vortices of strength $\Gamma(x)$ above the wing at positions $\pm y_v(x)$, $z_v(x)$. The strength $\Gamma(x)$ varies in streamwise direction and therefore in order to satisfy Kelvin's Law of Conservation of Circulation, feeding vortex sheets in the form of 'cuts' of strength $\frac{d\Gamma(x)}{dx}$ at the leading edges have been assumed. The axis of vorticity in these sheets is assumed to lie in the yz-plane and because slender wing conical flow is implied, the cuts do not affect the velocity profile in cross-flow plane.

It is noted that the component of free stream V in x-direction is $V\cos\alpha$ and in the cross-flow yz-plane, $V\sin\alpha$. Both components must be considered to obtain the velocity and pressure fields.

II.3 Camber Shape Transformations and their Properties

In order to make a satisfactory study by the slender body theory, it is necessary to find conformal transformation which transforms the camber line in the cross-flow plane $Z = y + iz$ into a circle or a vertical slit. For a general shape this cannot be done in closed form and in the present approach, the series of transformations as used by Maskell and Cooke - Ref.7 are employed. These are summarised as follows (see also Fig.5):

Transformations

$$Z = y + iz$$

$$Z_3^2 = Z^2 - 4c^2 \quad \text{or} \quad Z^2 = Z_3^2 + 4c^2 \tag{1}$$

$$Z_2 = Z_3 + 2ia\tan\delta \quad \text{or} \quad Z_3 = Z_2 - 2ia\tan\delta \tag{2}$$

$$Z_1 = \frac{Z_2}{2} \pm \frac{1}{2}\sqrt{Z_2^2 - 4a^2} \quad \text{or} \quad Z_2 = Z_1 + \frac{a^2}{Z_1} \tag{3}$$

$$Z_o = Z_1 - ia\tan\delta \quad \text{or} \quad Z_1 = Z_o + ia\tan\delta \tag{4}$$

$$T_e = Z_o - \frac{a_1^2}{Z_o} \quad \text{or} \quad Z_o = \frac{T_e}{2} \pm \frac{1}{2}\sqrt{T_e^2 + 4a_1^2} \tag{5}$$

$$T = T_e + 2ia_1\sin\delta \quad \text{or} \quad T_e = T - 2ia_1\sin\delta \tag{6}$$

These transformations leave the point at infinity unchanged.

It must be mentioned that the camber in Z-plane is generated on the assumption of a circular arc in the Z_3-plane.

The Transformation derivatives are given by the following relations

$$\left.\begin{aligned} \frac{dZ}{dZ_3} &= \frac{Z_3}{Z} \\ \frac{dZ_3}{dZ_2} &= 1 \\ \frac{dZ_2}{dZ_1} &= 1 - \frac{a^2}{Z_1^2} \\ \frac{dZ_1}{dZ_o} &= 1 \\ \frac{dZ_o}{dT_e} &= \frac{Z_o^2}{Z_o^2 + a_1^2} \\ \frac{dT}{dT_e} &= 1 \end{aligned}\right\} \quad (7)$$

We shall also require $\frac{d^2Z}{dT^2}/\frac{dZ}{dT}$ for the evaluation of Boundary Condition of zero force on Vortex-cut arrangement (Section II.6) and this is derived here.

From equations (7), we have

$$\frac{dZ}{dT} = \frac{dZ}{dZ_3} \cdot \frac{dZ_2}{dZ_1} \cdot \frac{dZ_o}{dT_e} \cdot$$

$$\therefore \quad \frac{d^2Z}{dT^2}/\frac{dZ}{dT} = \frac{d^2Z}{dZ_3 dT} \cdot \frac{dZ_3}{dZ} + \frac{d^2Z}{dZ_1 dT} \cdot \frac{dZ}{dZ_2} + \frac{d^2Z_o}{dT^2} \cdot \frac{dT}{dZ_o}$$

$$= \frac{1}{Z_3} \cdot \frac{dZ_3}{dT} - \frac{1}{Z} \cdot \frac{dZ}{dT} + \frac{2a^2}{Z_1^3} \cdot \frac{dZ_1}{dT} \cdot \frac{dZ_1}{dZ_2}$$

$$+ \frac{2a_1^2 Z_o}{(Z_o^2 + a_1^2)^2} \cdot \qquad (8)$$

If a point P on the circle is given by

$Z_o = a \sec\delta e^{i\lambda}$ $(= a_1 e^{i\lambda})$ and $Z_1 = re^{i\theta}$,

then it can be easily shown that

$$r^2 - a^2 = 2r.a.\tan\delta\sin\theta \qquad (9)$$

$$r = a\tan\delta\sin\delta + a\sqrt{1 + \tan^2\delta\sin^2\theta} \qquad (10)$$

and that

$$y_3 = 2a\cos\theta\sqrt{1 + \tan^2\delta\sin^2\theta}$$

$$z_3 = -2a\tan\delta\cos^2\theta.$$

If we write

$$\sin\phi = \sin\delta\cos\theta \qquad (11)$$

then we have

$$y_3 = R \sin 2\phi$$

$$z_3 = -R(1-\cos 2\phi)$$

where

$$R = 2a \operatorname{cosec} 2\delta.$$

Hence

$$Z_3 = 2R \sin\phi e^{-i\phi}, \qquad (12)$$

and ϕ is angle shown in Fig.2 and R is the radius of the circle in the Z_3-plane.

Family of Cross Section Shapes

There are simple relations between the various parameters of the drooped wing and these are derived here.

At the leading edge of the wing A where $\theta = 0$ and $\phi = \delta$, Z_3 and $Z = (+s - iHs)$ are related by

$$Z_3 = 2a \sec\delta e^{-i\delta}.$$

$$Z = (s - iHs)^2 = 4c^2 + 4a^2\sec^2\delta e^{-2i\delta}.$$

On separating real and imaginary parts, we get

$$s^2(1 - H^2) = 4c^2 + 4a^2(1 - \tan^2\delta) \qquad (13)$$

$$s^2H = 4a^2\tan\delta. \qquad (14)$$

At the shoulder point B where $Z_3 = 0$ and

$$y = 2c = ns. \qquad (15)$$

From equations (13), (14) and (15) we find

$$\frac{1 - H^2 - n^2}{H} = \frac{1-\tan^2\delta}{\tan\delta}$$

or

$$\cot 2\delta = \frac{1 - n^2 - H^2}{cH}.$$

Given n and H this determines δ and then c/a may be obtained from

$$\bar{c}^2 = \frac{c^2}{a^2} = \frac{n^2 \tan\delta}{H} .$$

It is useful at this stage to collect here for reference certain formulae which will be required later.

If $ds_\circ$ is an element of the arc of the circle, then

$$ds_\circ = a \sec\delta d\lambda = \{r^2 + (\frac{dr}{d\theta})^2\}^{\frac{1}{2}} d\theta = \frac{r}{\cos\phi} d\theta . \qquad (16)$$

For points on droops we have from equations (1) and (12)

$$2 Z (\frac{dy}{d\phi} + i\frac{dz}{d\phi}) = 8R^2 \sin\phi e^{-3i\phi}$$

or

$$\frac{dy}{d\phi} + \frac{idz}{d\phi} = \frac{4R^2 \sin\phi}{Ze^{3i\phi}} .$$

If we let

$$Z e^{3i\phi} = e_1 + if_1$$

then on the droops

$$\frac{dz}{dy} = - \frac{f_1}{e_1} . \qquad (17)$$

Now if ds is the element of arc on the droops we note that

$$\frac{ds}{d\phi} = \left|\frac{dy}{d\phi} + i\frac{dz}{d\phi}\right| = \frac{4R^2 \sin\phi}{|Z|} \qquad (18)$$

on the droop

$$\left|\frac{dz_2}{dz_1}\right| = \left|1 - \frac{a^2}{z_1^2}\right| = \left|1 - \frac{a^2}{r^2 e^{2i\theta}}\right| = \left|\frac{r^2 - a^2 e^{-2i\theta}}{r}\right|$$

$$= \frac{\sqrt{r^4 - 2a^2r^2\cos 2\theta + a^4}}{r^2} = \frac{\sqrt{(r^2-a^2)^2 + 4r^2a^2\sin^2\theta}}{r^2} \qquad (19)$$

$$= \frac{2a\sin\theta}{r\cos\delta}$$

using equation (9).

In many cases we shall consider δ so small that we may ignore δ^4 compared with unity.

We then have

$$|Z|^2 = 4a^2\{\bar{c}^4 + \frac{\cos^4\theta}{\cos^4\delta} + \frac{2\bar{c}^2\cos^2\theta}{\cos^2\delta}(1-2\sin^2\delta\cos^2\theta)\}^{\frac{1}{2}} \qquad (20)$$

$$= 4a^2(\bar{c}^2 + \cos^2\theta)\{1 + \frac{\delta^2(\cos^4\theta+\bar{c}^2\cos^2\theta-2\bar{c}^2\cos^4\theta)}{(\bar{c}^2+\cos^2\theta)^2}\}$$

Also

$$\mathcal{I}(Z^2 e^{3i\phi}) = \mathcal{I}\{e^{3i\phi}(4c^2+4R^2\sin^2\phi e^{-2i\phi})\} = 4(c^2\sin 3\phi + R^2\sin^3\phi). \qquad (21)$$

$$= 4a^2\{\bar{c}^2(3\sin\phi - 4\sin^3\phi) + \frac{\sin^3\phi}{\sin^2\delta\cos^2\delta}\}$$

$$= 4a^2\sin\delta\left[3\bar{c}^2\cos\theta + \cos^3\theta + \delta^2\cos^3\theta(1-4\bar{c}^2)\right] \ldots (22)$$

<u>The Normal Velocity on the Surface</u>

Since the surface of the wing is conical through origin O its equation must be homogenous in x,y,z and may be written

$$\frac{z}{kx} = f\left(\frac{y}{kx}\right)$$

and

$$\frac{\partial z}{\partial x} = k \quad f(y/kx) - \frac{y}{x} f'(y/kx)$$

$$= k\frac{z}{kx} - \frac{ky}{kx} \cdot \frac{dz}{dy}$$

$$= \frac{k}{se_1}(e_1 z + f_1 z)$$

using equation (17) and putting $kx = s$.

Hence

$$\frac{\partial z}{\partial x} = \frac{k}{se_1} \quad \{(e_1 + if_1)(y + iz)\}$$

$$= \frac{k}{se_1} \quad (z^2 e^{3i\phi}).$$

The velocity normal to the contour in the cross-flow plane due to the component $V\cos\alpha$ is on the "droops" (ref.7), see Fig.6.

$$\frac{\partial \phi}{\partial n} = v_n = \frac{V\cos\alpha \frac{\partial z}{\partial x}}{\{1 + (\frac{\partial z}{\partial y})^2\}^{\frac{1}{2}}} = \frac{V\cos\alpha . \frac{k}{se_1} . (Z^2 e^{3i\phi})}{\sqrt{1 + (f_1/e_1)^2}}$$

$$= \frac{k\ V\cos\alpha \quad (Z^2 e^{3i\phi})}{s|Z|} \qquad \ldots\ldots\ldots \qquad (23)$$

v_n is zero on the flat part of the section.

In order to find the complex velocity potential we shall need the component v_{n_o} in Z_o-plane which is related to v_n by the mapping ratio $\left|\frac{dZ}{dZ_o}\right|$. Using equations (1), (12), (19), (21) and (23) we find that

$$v_{n_o} = v_n \left|\frac{dz}{dz_o}\right|$$

$$= v_n \left|\frac{dz}{dz_3}\right| \left|\frac{dz_3}{dz_2}\right| \left|\frac{dz_2}{dz_1}\right| \left|\frac{dz_1}{dz_o}\right|$$

$$= \frac{k\ V \cos\alpha\, \vartheta(z^2 e^{3i\phi})}{s\,|z|} \cdot \left|\frac{z_3}{z}\right| \cdot \frac{2a \sin\theta}{r \cos\delta}$$

$$= \frac{16k\ V\, a^2 \cos\alpha\,(c^2 \sin^3\phi + R^2 \sin^3\phi)\sin\theta\cos\theta}{s \cos^2\delta \quad |z|^2 r} \quad \ldots\ldots (24)$$

Care must be taken with signs here. We adopt the convention that v_n represents the component of velocity along outward drawn normal. Therefore v_n is positive on upper surface and negative on the lower surface of the droops. v_{n_o} is zero at the leading edge.

II.4 The Complex Velocity Potential

The Complex Velocity potential W comprises the cross-flow and axial flow contributions. The cross flow contributions arise due to the freestream components V sinα, V cosα and the vortices $\pm\Gamma$ at $(\pm y_v, z_v)$. The axial contribution arises due to V cosα. This can be represented as

$$W = W_1(V \sin\alpha) + W_2(V \cos\alpha) + W_3(\Gamma) + W_4(x) \ldots\ldots\ldots \quad (25)$$

By virtue of transformation of the Z-plane to T_e-plane, W_1 and W_3 become

$$W_1 = -i\ V \sin\alpha . T_e \quad (26)$$

$$W_3 = -\frac{i\Gamma}{2\pi} \log \frac{T_e - T_{e_1}}{T_e + \bar{T}_{e_1}} \quad (27)$$

where T_{e_1} is the position of right hand vortex in the T_e-plane.

W_4 is simply written as

$$W_4 = V \cos\alpha . x. \tag{28}$$

W_2 arises for wings other than thin and flat and Weber (Ref.17) and Cooke (Ref.7) show that it is best represented in ζ_o-plane. W_2 is defined as the complex velocity potential required to produce a normal velocity v_{n_o} at the surface of the circle. It is equivalent to considering the effects of a source of strength $2\Pi . a_1 . \bar{v}_{n_o}$ at the centre of the circle together with a source distribution on the circumference of strength $2(v_{n_o} - \bar{v}_{n_o})$ per unit length, where $\bar{v}_{n_o}$ is the mean velocity on the circumference given by

$$\bar{v}_{n_o} = \frac{1}{2\pi} \int_o^{2\pi} v'_{n_o}(\lambda')d\lambda'. \tag{29}$$

For a thin wing it can be verified that $\bar{v}_{n_o}$ vanishes as expected.

Hence the complex velocity potential W_2 is given by

$$W_2 = \frac{1}{2\pi} \int 2v'_{n_o} \log (Z_o - Z'_o) ds'_o$$

$$= \frac{a_1}{\pi} \int_o^{2\pi} v'_{n_o} (\lambda') \log (Z_o - Z'_o)\, d\lambda' \tag{30}$$

where Z_o' is a point on the contour but Z_o is any point in the complex plane.

On the surface of the circle in Z_o-plane, following Weber[17], the velocity potential Φ_2 can be written as

$$\Phi_2 = (W_2) = \frac{a_1}{\pi} \int_o^{2\pi} v'_{n_o}(\lambda') \log |Z'_o - Z'_o| \, d\lambda' \tag{31}$$

we shall also need $\frac{dW_2}{dZ_o}$ for calculation of velocities. It follows from differentiation of equation (30)

$$\frac{dW_2}{dZ_o} = \frac{a_1}{\pi} \int_o^{2\pi} \frac{v'_{n_o}(\lambda') \, d\lambda'}{Z_o - Z'_o} = I_v(Z_o) \tag{32}$$

The reduction of integral $I_v(Z_o)$ is dealt with in Appendix A. This is interpreted as a Cauchy Principal Value integral and its value depends on whether the point Z_o lies on the surface of the circle or outside it, as follows:-

<u>Z_o on circle</u> $Z_o = a_1 e^{i\lambda}$

$$\frac{dW_2}{dZ_o} = I_v(Z_o) = \frac{a_1}{\pi} \int_o^{2\pi} \frac{v'_{n_o}(\lambda') - v_{n_o}(\lambda)}{Z_o - Z'_o} \, d\lambda' + \frac{a_1 \, v_{n_o}(\lambda)}{Z_o} \tag{33}$$

<u>Z_o outside circle</u> $Z_o = pe^{i\lambda}$, $p > a_1$

$$\frac{dW_2}{dZ_o} = I_v(Z_o) = \frac{a_1}{\pi} \int_o^{2\pi} \frac{v'_{n_o}(\lambda') - v_{n_o}(\lambda)}{Z_o - Z'_o} \, d\lambda' + \frac{2a_1 \, v_{n_o}(\lambda)}{Z_o} \tag{34}$$

Alternative forms for W_2 and its derivative $\frac{dW_2}{dZ_o}$ have been derived by Cooke[7]. He uses θ' as the integration variable instead of λ'. Using equations (16), (24) and (30), W can be written as

$$W_2 = C \int_o^{2\pi} B'(\theta') \log (Z_o - Z'_o) \, d\theta' \tag{35}$$

where

$$C = \frac{16 \, k.V \, a^2 \cos \alpha}{\pi s \cos^2 \delta} \tag{36}$$

$$B'(\theta') = \frac{(c^2 \sin 3\phi' + R^2 \sin^3 \phi') \sin\theta' \cos\theta'}{\cos\phi' |Z'|^2} \tag{37}$$

On the surface of the wing W_2 can be reduced to Φ_2 and evaluated exactly (Ref. 7 and 17) as shown in Appendix B.

The complex velocity derivative $\frac{dW_2}{dZ_o}$ is given by

$$\frac{dW_2}{dZ_o} = C \int_o^{2\pi} \frac{B'(\theta') \, d\theta'}{Z_o - Z'_o} \tag{38}$$

Equation (20) on substitution of equations (21), (22) and (23) becomes

$$W(T_e) = -iV \sin\alpha \, . \, T_e - \frac{i\Gamma}{2\pi} \log \frac{T_e - T_{e_1}}{T_e + \overline{T}_{e_1}} + W_2 + V \cos\alpha . x \tag{39}$$

with W_2 given by either equation (30) or (35).

The complex velocity derivative $\frac{dW}{dZ}$ is given by

$$\frac{dW}{dZ} = \frac{dW}{dT_e} \cdot \frac{dT_e}{dZ} = - iV\sin\alpha \cdot \frac{dT_e}{dZ} - \frac{i\Gamma}{2\pi}\left(\frac{1}{T_e - T_{e_1}} - \frac{1}{T_e + \overline{T}_{e_1}}\right)\frac{dT_e}{dZ} + \frac{dW_2}{dZ_o} \cdot \frac{dZ_o}{dZ} \qquad (40)$$

with $\frac{dW_2}{dZ_o}$ given by either equation (33) or (34) or (38).

II.5 The Boundary Condition of Finite Velocity at the Leading Edge

This condition is applied in the cross-flow plane at the leading edge ($Z = s - i\,Hs$, $Z_o = a_1 e^{-i\delta}$). The complex velocity derivative $\frac{dW}{dZ}$ is non singular at the leading edge. Using equation (39), we obtain

$$\frac{dW}{dZ} = iV\sin\alpha \cdot \frac{dT_e}{dZ} - \frac{i\Gamma}{2\pi}\left(\frac{1}{T_e - T_{e_1}} - \frac{1}{T_e + \overline{T}_{e_1}}\right) \cdot \frac{dT_e}{dZ} + \frac{dW_2}{dZ_o} \cdot \frac{dZ_o}{dZ} \qquad (41)$$

where

$$\frac{dZ_o}{dZ} = \frac{dZ_o}{dZ_1} \cdot \frac{dZ_1}{dZ_2} \cdot \frac{dZ_2}{dZ_3} \cdot \frac{dZ_3}{dZ} = \frac{dZ_1}{dZ_2} \cdot \frac{dZ_3}{dZ}$$

$$\frac{dT_e}{dZ} = \frac{dT_e}{dZ_o} \cdot \frac{dZ_o}{dZ}$$

At the leading edge $\frac{dZ_1}{dZ_2}$ is infinite, although other derivatives of the transformations are finite. Hence for finite $\frac{dW}{dZ}$ at the leading edge, we must have $\left(\frac{dW}{dT_e}\right)_{L.E.} = 0$

$$\left(\frac{dW}{dT_e}\right)_{L.E.} = \left[- iV\sin\alpha - \frac{i\Gamma}{2\pi}\left(\frac{1}{T_e - T_{e_1}} - \frac{1}{T_e + \overline{T}_{e_1}}\right) + \frac{dW_2}{dZ_o} \cdot \frac{d\overline{Z_o}}{dT_e}\right]_{L.E.} = 0$$

or

$$iV\sin\alpha = \frac{i\Gamma}{2\pi} \cdot \frac{T_{e_1} + \overline{T}_{e_1}}{T_{e_1}\,\overline{T}_{e_1}} + \alpha_D \left(\frac{dZ_o}{dT_e}\right)_{L.E.} \qquad (42)$$

where

$$\alpha_D = \left(\frac{dW_2}{dZ_o}\right)_{L.E.}$$

and

$$\left(\frac{dZ_o}{dT_e}\right)_{L.E.} = \left(\frac{Z_o^2}{Z_o^2 + a_1^2}\right)_{L.E.}$$

α_D can be obtained directly from equation (33) by numerical integration or from the exact method outlined in Appendix C.

II.6 The Boundary Condition of Zero Force on the Vortex-cut.

The condition of zero force on the vortex-cut combination follows directly from Brown and Michael (8) and can be written as

$$(v_1 + iw_1)_{Z=Z_V} = \frac{V}{x}(2Z_V - Z_L)$$

or

$$(v_1 - iw_1)_{Z=Z_V} = \frac{V}{x}(2\bar{Z}_V - \bar{Z}_L) \qquad (43)$$

where $v_1 + iw_1$ is the velocity at the right-hand vortex and is found by subtracting the velocity field of the vortex at Z_V from the total velocity and taking the limit as $Z \to Z_V$.

Using equation (38), the complex velocity potential W_1 at the right-hand vortex is written as

$$W_1 = W + \frac{i\Gamma_1}{2\pi} \log(Z-Z_V) \qquad (44)$$

and by differentiating with respect to Z and taking the limit as $Z \to Z_V$, we obtain

$$\left[\frac{dW_1}{d\bar{Z}}\right]_{Z\to Z_V} = v_1 - iw_1$$

i.e.

$$\left[\frac{dW_1}{d\bar{Z}}\right]_{Z\to Z_V} = \left[\left\{-iV\sin\alpha - \frac{i\Gamma}{2\pi}\left(\frac{1}{T_e - T_{e_1}} - \frac{1}{T_e + \bar{T}_{e_1}}\right)\right\}\frac{dT}{d\bar{Z}} + \frac{i\Gamma}{2\pi}\frac{1}{\bar{Z}-\bar{Z}_V}\cdot\right.$$

$$\left. + \left(\frac{dW_2}{dZ_o}\cdot\frac{dZ_o}{d\bar{Z}}\right)_{Z\to Z_V}\right.$$

with $\frac{dW_2}{dZ_o}$ given by either equation (34) or (37).

Substituting equation (35) for $V \sin\alpha$, we have,

$$v_1 - iw_1 = \left[-\frac{i\Gamma}{2\pi} \frac{T_e + T_{e_1}}{T_e \cdot \bar{T}_{e_1}} - \alpha_D \frac{dZ_o}{d\theta}(LE) - \frac{i\Gamma}{2\pi} \left[\left\{ \frac{1}{T_e - T_{e_1}} - \frac{\frac{dZ}{dT_e}}{Z - Z_1} \right\} - \frac{1}{T_e + \bar{T}_{e_1}} \right] \frac{dT_e}{dZ} \right.$$

$$\left. + \left(\frac{dW_2}{dZ_o} \cdot \frac{dZ_o}{dZ} \right)_{Z \to Z_V} \right. \tag{45}$$

Now by using L'Hospital's rule it can be shown that

$$\left\{ \frac{1}{T_e - T_{e_1}} - \frac{\frac{dZ}{dT_e}}{Z - Z_V} \right\} = \varepsilon_1 = -\frac{1}{2} \left[\frac{\frac{d^2 Z}{dT_e^2}}{\frac{dZ}{dT_e}} \right]_{T_e = T_{e_1}}$$

and equation (8) may be substituted here.

From equation (45), we can write the vortex strength Γ as

$$\Gamma = \frac{\frac{V}{X}(2\bar{Z}_v - \bar{Z}_L).2\pi i + \alpha_D \frac{dZ_o}{d\bar{T}_e} .2\pi i - \alpha_V \frac{dZ_o}{d\bar{T}_e} . 2\pi i}{\left\{ \frac{T_{e_1} + T_{e_1}}{T_{e_1} \cdot \bar{T}_{e_1}} + \varepsilon_1 - \frac{1}{T_e + \bar{T}_{1e}} \right\} \frac{dT_e}{dZ}} \tag{46}$$

where

$$\alpha_V = \left(\frac{dW_2}{dZ_o} \cdot \frac{dZ_o}{dZ} \right)_{Z \to Z_V} \tag{47}$$

The complex equation (46) now gives a complex value for the vortex strength for a given position of the vortex . The procedure we follow is to fix the height of the vortex and vary the spanwise position until Γ has zero imaginary part. The angle of incidence then follows directly from equation (42). This procedure is based on Reference 8.

II.7 Pressure Distribution and Forces

Pressure Coefficient

The pressure coefficient to the same order as the linearized equation for the potential is given for slender configurations by

$$Cp = \sin^2\alpha - 2\frac{\Phi x}{V}\cos\alpha - \frac{1}{V^2}(\Phi_y^2 + \Phi_z^2)$$

where

$$\Phi = \Phi(x, y, z) = \mathcal{R}\{W\}.$$

In conical flow Φ may be written as

$$\Phi = x.\Phi_x + y.\Phi_y + z.\Phi_z + \mu \text{ (a constant)}$$

The differentiation with respect to x is for constant y and z, i.e. constant Z, so that

$$\Phi_x/k = \mathcal{R}\{W\} - y\mathcal{R}\left\{\frac{dW}{dZ}\right\} - z\,\mathcal{I}\left\{\frac{dW}{dZ}\right\}.$$

It follows then that

$$Cp = \sin^2\alpha - \frac{2k}{V}\left[\left\{\mathcal{R}(W) - y\mathcal{R}\left\{\frac{dW}{dZ}\right\} - z\,\mathcal{I}\left\{\frac{dW}{dZ}\right\}\right]\cos\alpha\right.$$

$$\left. - \frac{1}{V^2}\left[\left\{\mathcal{R}\left(\frac{dW}{dZ}\right)\right\}^2 + \left\{\mathcal{I}\left(\frac{dW}{dZ}\right)\right\}^2\right] + \frac{2\mu}{V_x}\right.$$

W and $\frac{dW}{dZ}$ follow from equation (39) and (40). The constant μ must be chosen so that Cp vanishes as $y, z \to \infty$.

On the surface of the wing the part of the complex potential due to drooped leading edges (W_2) presents some problem and care must be taken in its evaluation. In Appendix B, a method for reduction of W_2 to Φ_2 based on Refs 7 and 17 has been given.

Similarly, care must be exercised in evaluation of $\frac{dW_2}{dZ}$. The Cauchy Principal value integral is implied and numerical integration procedure should account for this.

The lift force coefficient C_L based on the projected area of the wing s^2/k is given by combining the linear lift expression of Ref.7 with the non-linear lift due to the vortices (e.g. Ref.15)

$$\frac{C_L}{\cos^2\alpha} = \Pi k^2 \cdot 4\left(\frac{a}{s}\right)(2+2\bar{c}^2+\tan^2\delta)\frac{\sin\alpha}{k}$$

$$- 4\left(\frac{a}{s}\right)^3\frac{\tan\delta}{\cos^2\delta} \cdot \cos\alpha\,(M-\delta^2 N) + 2 \cdot \frac{\Gamma}{Vs} \cdot (T_{el}+\bar{T}_{el}),$$

where
$$M = 1 + 8\bar{c}^2 + 16\bar{c}^4 - 16\frac{\bar{c}^2}{h} - \frac{16\bar{c}^4}{h},$$

$$N = 2\left(5\bar{c}^2 + 8\bar{c}^4 - 40\bar{c}^6 - 14\frac{\bar{c}^2}{h} + 12\frac{\bar{c}^4}{h} + 40\frac{\bar{c}^6}{h} + \frac{2}{h^3}\right).$$

The lift and induced drag coefficients C_L and C_D may also be obtained from integration of pressures on the wing as follows

Forces

We define the conical wing surface by the equation

$$F(x,y,z) \equiv z - kx\, f\left(y/kx\right) = 0$$

Unit normal vector $\underline{\hat{n}}$ defining the surface is given by

$$\underline{\hat{n}} = \frac{\underline{i}\,F_x + \underline{j}\,F_y + \underline{k}\,F_z}{\{F_x^2 + F_y^2 + F_z^2\}^{\frac{1}{2}}}$$

where
$$F_x = - k\, f\left(y/kx\right) + y/x\, f'\left(y/kx\right)$$

$$= - k\left(z/kx\right) + k\left(y/kx\right) dz/dy$$

$$F_y = - k_x\, f'\left(y/kx\right).\frac{1}{kx} = f'\left(y/kx\right) = dz/dy$$

$$F_z = 1$$

We also define

$$F_r = \{F_x^2 + F_y^2 + F_z^2\}^{\frac{1}{2}}$$

The Force vector $\underline{dF}$ is defined by

$$\underline{dF} = Cp \; d \; S \; \hat{\underline{n}}$$

where d S is an elemental surface area. This is can be represented in terms of arc length d σ as

$$dS = \frac{1}{2} \cdot x \cdot d\sigma \text{ for a conical wing of centre line chord x.}$$

$$d\sigma = dy^2+dz^2 = dy^2 \left(1 + \frac{dz}{dy}\right)^2 = dy^2 \{1 + f'^2\}$$

The force coefficients C_x and C_{z_o} in x and z directions respectively are then given by

$$C_x = \frac{2}{k_x^2} \cdot \int_{y=-s}^{y=s} \underline{i} \; \underline{dF} = \frac{2}{k_x^2} \int_{y=-s}^{y=s} Cp.dS. \frac{F_x}{F_r}$$

$$= \int_{-1}^{1} Cp \; \frac{(1+f'^2)^{\frac{1}{2}} \; (-k1+y/_x f')}{F_r} \; d \; (y/_{kx})$$

and

$$C_z = \frac{2}{k_x^2} \int_{y=-s}^{y=s} \underline{k} \; \underline{dF} = \frac{2}{k_x^2} \int_{y=-s}^{y=s} Cp \; dS \; \frac{F_z}{F_r}$$

$$= \int_{-1}^{+1} Cp \; \frac{(1+f')^2}{F_r} \; d \; (y/_{kx})$$

Lift coefficient C_L and drag coefficient C_D follow by resolving the force coefficients C_x and C_z.

$$C_L = C_z \cos \alpha - C_x \sin \alpha$$

$$C_D = C_z \sin \alpha + C_x \cos \alpha$$

It must be mentioned that although the above derivations are generally applicable, in this report we have not included viscous effects.

III RESULTS

The type of camber lines generated by the method are shown in Fig. 7. The angle of droop measured at the leading-edge increases as the shoulder position moves outboard.

For each configuration, there are two particular incidences α_0 and α_s. α_0 corresponds to zero lift and α_s to the attitude where the load at the leading edge vanishes. For an uncambered wing α_0 and α_s both coincide at 0^0. However, for a wing with leading edge droop, both α_0 and α_s will be positive.

Strictly speaking the value of α_0 depends on the method of solution of the problem i.e. if the flow is assumed to be separated as in present theory or if it is attached. The difference in practice for "realistic" configurations is however likely to be very small. α_0 therefore may be calculated easily.

The angle α_s has a special significance, it indicates the side of the wing on which the leading edge vortex lies. For $\alpha > \alpha_s$ the leading edge vortex lies above the upper surface and vice-versa.

Fig. 8 depicts the variation of $\sin\alpha_s/k$ for a set of camber lines. As might be expected, α_0 increases both with increasing amount of droop and as the shoulder position approaches the leading edge.

As mentioned in the Introduction, previous work contains adequate reference to uncambered and circular camber wings (zero shoulder position). The emphasis in this report is therefore on the aerodynamic effects as the shoulder position moves out toward the leading edge. Both attached and separated flow solutions have been considered.

III.1 Attached Flow

In general, the Attached Flow theory applied for small incidences only. Fig. 9 shows the effect of shoulder position on C_L at fixed incidences for two values of camber parameter H = 0.05s and 0.1s. It is noted that, in general, as incidence increases the effect due to a fixed droop decreases. When the shoulder of the droop tends to the leading edge, there is a gain in lift, although for most part droop causes a reduction in lift at a particular attitude.

In Fig. 10 pressure distributions are shown at 5^o incidence (k = .25) for various shoulder positions. It is interesting to note the oscillatory behaviour of the pressures near the leading edge on the upper surface as the shoulder moves outboard from .775s to .875s.

Such a behaviour is also likely to arise for some other droop configuration at a different incidence. It also illustrates the problem of determining C_L and C_D from C_p distribution by numerical integration. A large number of sampling points may be required near the leading edge.

III.2 Separated Flow

Figs. 11 and 12 show a selection of results as the shoulder position of the droop is varied. The camber parameter values considered are $H = .05s, .10s$. In each case the following relationships have been presented:

(i) vortex locus.

(ii) vortex height $(z_v + H)/s$ against α.

(iii) vortex strength $\frac{\Gamma}{Vs}$ against α.

(iv) C_L against α

Constant C_L or α lines where appropriate have been interpolated.

For shoulder positions less than .9s, we infer:-

(i) vortex locus moves outwards both with increasing shoulder position and camber.

(ii) For a given shoulder position, the vortices move closer to the surface as camber increases.

(iii) For a given camber, as the shoulder moves outwards the vortex strength decreases at a fixed incidence. This is particularly noted at smaller incidences. At higher incidence the curves approach the flat wing case.

(iv) For a given camber, as the shoulder moves outward, the lift decreases at a particular incidence, the tendency being more marked at lower incidences.

An interesting feature of results is that for shoulder positions very near the leading edge, the vortex height is apparently multi-valued through a small incidence range (e.g. for configuration with n ≈ .95s, H = .05s and $10.0^{\circ} < \alpha < 15.0^{\circ}$). Lift~incidence and vortex strength ~ incidence relationships also exhibit a similar tendency. The solution therefore admits the possibility of up to three different flow-fields. Fig.13 showsthe three types of pressure distributions corresponding to three vortex positions - "low", "intermediate" and "high" at $\alpha \triangleq 11.7^{\circ}$. The span-wise variation of the velocity tangential to the upper surface in the cross-flow plane is shown in Fig.14. for all three vortex positions. The curves indicate that reattachment streamlines which enclose the separation and then split in two ways impinge on the wing for the "low" and "intermediate" vortex positions (vis. .98s and .85s respectively) but not for the "high" vortex position. Flow patterns as sketched in Fig.15 are indicated. The flow patterns also show general agreement with the features of pressure distributions. For the "low" vortex position the peak suction appears outboard of the shoulder. For the "intermediate" and "high" vortex position the peak suctions occur near and inboard of the shoulder position respectively.

This analysis leads to the question of what happens in experimental flows where the results are not likely to be multiple-valued for a given configuration and there would be a preferred flow field. Two possible explanations may be advanced as follows:-

(i) The preferred flow-field would depend on the shape of the wing plan form near the section under consideration. If the sweepback decreases aft of the section under consideration (as in Fig.16(a)) the tendency may be towards attached flow type of flow field e.g. either for "low" or "intermediate" position. Conversely, if the sweepback increases aft of the section under consideration, then the tendency may be for "high" position flow field. (Fig.16(b))

(ii) The velocities on the wing surface for the "low" and "intermediate" vortex positions are fairly large near the leading edge. It is therefore not difficult to visualise the existence of multiple vortex system as sketched in Fig. 17.

Of the above two explanations, the latter one seems very plausible and experimental evidence indicates the presence of a number of vortex systems. This however suggests that the theoretical approaches generally used for design work which simulate only one separation system are not likely to be adequate. This criticism applied equally to conical and non-conical or lifting surface approaches.

It must be mentioned that Levinsky and Wei (17) also show the existence of multiple separations on slender bodies with Strakes (Fig.18). Their model however deals with only one separation. Additional criteria based on the development of the boundary layer on the body will be required to fix the strength and position of the second separation.

Comparisons at Constant C_L.

It is of interest to compare various quantities for a given C_L. Taking for example a value of $C_L = 0.3$, we look at the effect of droop shoulder position keeping the height of camber a constant at $H = .05s$. The results are shown in Fig. 19 and 20 we note the following as droop shoulder position increases:

(i) linear part if lift increases and the non-linear part decreases.

(ii) induced drag decreases and then increases again.

(iii) incidence required at the centre line increases.

(iv) The vortices move closer towards the leading edge.

(v) Up to shoulder position of 0.85s, the peak suction pressure on the upper surface increases and also its position moves outwards signifying a drag reduction acting on the drooped leading edge.
For shoulder position 0.95s, the suction peak is much smaller and this corresponds to a slight increase in lift induced drag.

To enable general conclusions to be drawn, this type of analysis needs to be carried out for a number of droop configurations.

Lift Dependent Drag Factor k_1

The variation of lift dependent drag factor $k_1 = \frac{\pi A C_{Di}}{C_L^2}$ at various lift coefficients for a representative series of wings with leading edge droop has been considered.

Wings with Circular-arc Cambers n = 0

Figure 21 shows the variation of the factor k_1 for leading edge droop up to 0.4s. It is noted that the factor k_1 reduces with increasing C_L. The discontinuities in the curves near low C_L values occur near the attachment angles of attack. The values for k_1 without leading edge singularity based on Smith's[5] results are shown for reference. Flow separation, therefore, is beneficial and gives a reduction in k_1.

Figure 22 shows a comparison between Barsby's[14] results with vortex sheet separation model and the present approach. It is interesting to note that at lower values of C_L, the present approach gives lower values for k_1 but for higher values it predicts higher values. The correspondence of the two methods improves with increasing camber.

Wings with Leading Edge Droop

The variation of shoulder position for leading edge droop of 0.05s and 0.1s has been depicted in Figures 23 and 24. It is noted that moving the shoulder of the camber outwards means a reduction in k_1.

For a given shoulder position at 0.8s the effect of leading edge droop has been shown in Figure 25. It is noted that increased droop is generally beneficial, but it may lead to a limiting value for droop. Further work can be done on this aspect to optimise the leading edge droop geometry for given C_L.

IV CONCLUSIONS AND RECOMMENDATIONS

In this report, slender body theory with exact boundary condition has been used to calculate the flows past a thin conically cambered wing (i.e. with drooped leading edges). The flow separation has been modelled as a vortex-cut arrangement.

Calculated results suggest that leading edge droop has a very marked effect on the local pressures near the leading edges and hence the overall aerodynamic forces. In particular, the lift-drag ratio can be enhanced by suitable choice of leading edge droop. The calculations need to be generalised for a set of cambers.

The results indicate a multiple valued solution for realistic cambers i.e. when the shoulder of the droop is very near the leading edge. In experiment, this is not likely and another separation system may exist near the high curvature wing-section. The work in this report therefore points to inadequacy of current design approaches with simulation of one vortex system only.

The method of this report may also be extended (see Fig. 26) to incorporate thin extensions of wing span, leading edge devices, secondary vortices and variation of separation points, cross-section thickness may also be included. More realistic vortex sheet representation (Ref.13) may also be incorporated.

From the point of view of aircraft manoeuverability, wing root gaps or leading edge gaps may also need to be studied. Asymmetrical configurations are also of interest.

APPENDIX A

Evaluation of Integral $I_v(Z_o)$

From Equation (27) we have

$$I_v(Z_o) = \frac{a_1}{\pi} \int_o^{2\pi} \frac{v_{n_o}(\lambda')\, d\lambda'}{Z_o - Z_o'}$$

$$= \frac{a_1}{\pi} \int_o^{2\pi} \frac{v_{n_o}(\lambda') - v_{n_o}(\lambda)}{Z_o - Z_o'} d\lambda' + \frac{a_1}{\pi} v_{n_o}(\lambda) \int_o^{2\pi} \frac{d\lambda'}{Z_o - Z_o'}$$

$$= \frac{a_1}{\pi} \int_o^{2\pi} \frac{v_{n_o}(\lambda') - v_{n_o}(\lambda)}{Z_o - Z_o'} d\lambda + a_1 v_{n_o}(\lambda) \cdot I_u(Z_o)$$

It is noted that the value of $I_u(Z_o)$ depends on whether Z_o lies on the surface of the circle or outside. It can be evaluated as follows:-

$$I_u(Z_o) = \frac{1}{\pi} \int_o^{2\pi} \frac{d\lambda}{Z_o - Z_o'}$$

$$= \frac{1}{\pi} \int_o^{2\pi} \frac{1}{Z_o - Z_o'} \cdot \frac{d\lambda}{dZ_o'} \cdot dZ_o'$$

Now $Z_o = a_1 e^{i\lambda}$ therefore we see $\frac{d\lambda'}{dZ_o'} = -\frac{i}{Z_o'}$

$$I_u(Z_o) = -\frac{i}{\pi} \int_o^{2\pi} \frac{dZ_o'}{(Z_o - Z_o')Z_o'} = -\frac{i}{\pi Z_o} \int_o^{2\pi} \left[\frac{1}{Z_o'} - \frac{1}{Z_o - Z_o'}\right] dZ_o'$$

If Z_o lies on the surface of the circle then

$$I_u(Z_o) = -\frac{i}{\pi Z_o} (2\pi i - \pi i) = \frac{1}{Z_o}$$

If Z_o lies outside the circle then

$$I_u(Z_o) = -\frac{i}{Z_o} (2\pi i - 0) = \frac{2}{Z_o}$$

APPENDIX B

The reduction of W_2 to Φ_2 and evaluation.

$$W_2 = C \int_0^{2\Pi} B' \log (Z_o - Z_o')d\theta'.$$

Denoting the real part of W_2 by Φ_2 we have

$$\Phi_2 = C \int_0^{2\Pi} B' \log |Z_o - Z_o'|d\theta'.$$

In the Z_o-plane if Φ_2 is to be evaluated at a point outside the circle, the integral presents no problem. However, on the surface, special care is required to deal with $\log|Z_o - Z_o'|$ term.

If we denote the radius of the circle by d then we have

$$\Phi_2 = C \int_{-\Pi/2}^{\Pi/2} B \log|y_o + iz_o - y_o' - iz_o'||y_o + iz_o + y_o' - iz_o'|$$

from the symmetry about the z_o-axis. Hence on the circle

$$\Phi_2 = \frac{C}{2} \int_{-\Pi/2}^{\Pi/2} B' \log\left[(y_o - y_o')^2 + (z_o - z_o')^2\right]\left[(y_o + y_o')^2 + (z_o - z_o')^2\right]d\theta'$$

$$= \frac{C}{2} \int_{-\Pi/2}^{\Pi/2} B' \log 4\left\{(d^2 - z_o z_o')^2 - y_o^2 y_o'^2\right\}d\theta' .$$

Putting $y_o^2 = d^2 - z_o^2$ we have

$$\Phi_2 = C \int_{-\Pi/2}^{\Pi/2} B' \log 2d|z_o - z_o'|\, d\theta'$$

on the surface of the section.

Since $z_o - z_o' = z_1 - z_1'$ we have on the surface, taking note of the signs of B'

$$\Phi_2 = C \int_{O}^{\Pi/2} B' \log \left| \frac{z_1 - z'_{1u}}{z_1 - z'_{1\ell}} \right| d\theta' \qquad (A1)$$

where z_{1u} is value of z_1' at a point specified by θ' and $z_{1\ell}'$ is its value at the corresponding point on the lower surface specified by $-\theta'$.

Given $\sin\psi = \frac{\tan\Phi}{\tan\delta}$, $\sin\phi = \sin\delta\cos\theta$

we have

$$\cos\theta = \frac{\sin\psi}{G} , \qquad \sin\theta = \frac{\cos\psi\sin\delta}{G}$$

$$\cos\Phi = \frac{\cos\delta}{G} \qquad \sin\Phi = \frac{\sin\psi\sin\delta}{G}$$

$$G^2 = 1 - \cos^2\psi\sin^2\delta.$$

and

$$r = a \tan\delta\sin\theta \quad a\sqrt{1 + \tan^2\delta s}$$

$$= a/G.(1 + \sin\delta\cos\psi)$$

$$\underline{r} = a/G.(1 - \sin\delta\cos\psi)$$

$$r\underline{r} = a^2$$

we have

$$z_1 = r \sin\theta = \frac{a \cos\delta\cos\psi}{1-\cos\psi\sin\delta}$$

$$z'_{1u} = r'\sin\theta' = \frac{a \cos\delta\cos\psi'}{1-\cos\psi'\sin\delta}$$

$$z'_{1_\ell} = -\underline{r}'\sin\theta' = -\frac{a \cos\delta\cos\psi'}{1+\cos\psi'\sin\delta}$$

and $$d\theta = -\frac{\cos^3 \cos\psi}{\cos\delta\sin\theta}\, d\psi.$$

On substitution, the log term in equation (A1) becomes

$$\log\left|\frac{z_1-z'_{1u}}{z_1-z'_{1_\ell}}\right| = \log\left|\frac{\left(\frac{\cos\psi}{(1-\cos\psi\sin\delta)} - \frac{\cos\psi'}{(1-\cos\psi'\sin\delta)}\right)}{\frac{\cos\psi}{1-\cos\psi\sin\delta} + \frac{\cos\psi'}{1+\cos\psi'\sin\delta}}\right|$$

$$= \log\left|\frac{\cos\psi-\cos\psi'}{\cos\psi+\cos\psi'} \times \frac{1+\cos\psi'\sin\delta}{1-\cos\psi'\sin\delta}\right|$$

$$= \log\left|\frac{\cos\psi-\cos\psi'}{\cos\psi+\cos\psi'}\right| + \log\left|\frac{1+\cos\psi'\sin\delta}{1-\cos\psi'\sin\delta}\right|$$

Φ_2 now becomes

$$\Phi_2 = C\int_0^{\Pi/2} B'\left|\log\left|\frac{\cos\psi-\cos\psi'}{\cos\psi+\cos\psi'}\right| + \log\left|\frac{1+\cos\psi'\sin\delta}{1-\cos\psi'\sin\delta}\right|\right| d\theta'$$

$$= C\left|I_A + I_B\right|$$

where

$$I_A = \int_0^{\Pi/2} B' \log\left|\frac{\cos\psi-\cos\psi'}{\cos\psi+\cos\psi'}\right| d\theta'$$

and

$$I_B = \int_0^{\Pi/2} B' \log\left|\frac{1+\cos\psi'\sin\delta}{1-\cos\psi'\sin\delta}\right| d\theta'.$$

If $B'd\theta'$ is now put in the form

$$B'd\theta' = -\frac{1}{4}\tan\delta\cos^2\delta\ g(\psi')d\psi'$$

where

$$g(\psi') = -B'd\theta'.\frac{4}{\tan\delta\cos^2\delta}.\frac{d\psi'}{d\psi'}$$

then

$$I_A = -\frac{1}{4}\tan\delta\cos^2\delta \int_{\Pi_2}^{o} g(\psi')\ \log\left|\frac{\cos\psi-\cos\psi'}{\cos\psi+\cos\psi'}\right|\ d\psi'.$$

Now $g(\Pi-\psi') = -g(\psi')$

therefore

$$I_A = \frac{1}{4}\tan\delta\cos^2\delta \int_{o}^{\Pi} g(\psi')\log|\cos\psi-\cos\psi'|\ d\psi'.$$

I_B may also be reduced in similar way

$$I_B = \frac{1}{4}\tan\delta\cos^2\delta \int_{o}^{\Pi/2} g(\psi')\log\left|\frac{1+\cos\psi'\sin\delta}{1-\cos\psi'\sin\delta}\right|\ d\psi'.$$

Φ_2 is now given by

$$\Phi_2 = C\left|\frac{1}{4}\tan\delta\cos^2\delta\,(J_A(\psi) + J_B)\right|$$

where $J_A(\psi) = \int_{o}^{\Pi} g(\psi')\ \log|\cos\psi-\cos\psi'|d\psi'$

$$J_B = \int_{o}^{\Pi/2} g(\psi')\log\left|\frac{1+\cos\psi'\sin\delta}{1-\cos\psi'\sin\delta}\right|\ d\psi'\ .$$

The value of $J_A(\psi)$ depends on ψ but J_B is a constant for a given wing and may be calculated by numerical integration.

Evaluation of $J_A(\psi)$

$$J_A(\psi) = \int_0^{\Pi} g(\psi') \log|\cos\psi - \cos\psi'| \, d\psi'.$$

This evaluation of thin form of integrals has been discussed by Weber (17) and a solution using Fourier Series is suggested. We know that $g(\psi)$ is an odd function which also gives $g(\psi'=0) = g(\psi'=\Pi/2) = g(\psi'=\Pi) = 0$ we write

$$g(\psi') = \sum_{\nu=1,3,5}^{N-1} b_\nu \cos\nu\psi' \qquad \text{(N even)}$$

$$J_A = \sum_{\nu=0,2}^{N} \int_0^{\Pi} \cos\nu\psi' \log|\cos\psi - \cos\psi'| \, d\psi$$

$$= \Pi \sum_{\nu=1}^{N} \frac{b_\nu}{\nu} \cos\nu\phi.$$

The coefficients b_ν are calculated from

$$b_\nu = \frac{2}{N} \sum_{\mu=0,1,2}^{N} g(\psi_\mu).\cos\nu\psi_\mu \qquad \text{(N even)}$$

$$(\nu=1,3,5\ldots N-1)$$

$$\psi_\mu = \frac{\mu\Pi}{N} \quad . \qquad \text{(N even)}$$

$$(\mu=0,1,2\ldots N)$$

APPENDIX C

Calculation of α_D - Exact Method

From Equations (38) and (41)

$$\alpha_D = \left[\frac{dW_2}{dZ_o}\right]_{L.E.} = \left[C\int_o^{2\pi} \frac{B'(\theta')d\theta'}{Z_o - Z_o'}\right]_{L.E.}$$

At the leading edge $Z_o = \frac{a_1 e^{-i\delta}}{\cos\delta}$, $Z_o - Z_o' = Z_1 - Z_1' = a - r'e^{i\theta'}$

Therefore

$$\alpha_D = C\int_o^{\pi/2} \left\{\frac{1}{a - r'e^{i\theta'}} - \frac{1}{a - \underline{r}e^{-i\theta'}} + \frac{1}{a - r'e^{i(\pi-\theta')}} - \frac{1}{a - \underline{r}'e^{-i(\pi-\theta')}}\right\} d\theta' .$$

Where $\underline{r}'$ is value of r' when θ' is replaced by $-\theta'$ we find that

$$\alpha_D = C\int_o^{\pi/2} B' \left\{\frac{2ie^{i\delta}\cos\phi'}{a\sin\theta'}\right\} d\theta'$$

Using equations (9), (10) and (11), and noting that

$$\left.\begin{aligned} r' - \underline{r}' &= 2a \tan\delta \sin\theta' \\ r' + \underline{r}' &= 2a \sec\delta \cos\phi' \\ r'\underline{r}' &= a^2. \end{aligned}\right\}$$

$$\alpha_D = C\int_0^{\pi/2} \frac{(c^2 \sin 3\phi' + R^2 \sin^3\phi')\cos\theta}{|Z'|^2} \times \frac{2ie^{i\delta}}{a}\, d\theta'$$

$$= C \cdot \frac{2ie^{i\delta}}{a} \cdot I_1$$

where

$$I_1 = \frac{1}{\pi}\int_0^{\pi/2} \frac{(c^2 \sin 3\phi' + R^2 \sin^3\phi')\cos\theta}{|Z'|^2}\, d\theta'$$

Using equation (36) we obtain

$$\alpha_D = 32Vi \cos\alpha . e^{i\delta} . \frac{k.a.}{s \cos^2\delta} . I_1 .$$

Equation (35) becomes

$$i\, V \sin\alpha = \frac{i\Gamma}{2\pi}\left(\frac{T_{1e} + \bar{T}_{1e}}{T_{1e}.\bar{T}_{1e}}\right) + 32iV \cos\alpha\, e^{i\delta} \frac{k.a.}{s \cos^2\delta} . I_1 . \left(\frac{e^{-2i\delta}}{e^{-2i\delta}+1}\right)$$

The integral I_1 has been evaluated in Ref.7 as

$$I_1 = \frac{\sin\delta}{16}\left[1 + 4\bar{c}^2 - \frac{4\bar{c}^2}{h} - \delta^2\left(6\bar{c}^2 - 8\bar{c}^4 - \frac{2\bar{c}^2}{h} + 8\frac{\bar{c}^4}{h} - \frac{4}{h^3} + \frac{3}{h^5}\right)\right.$$

where $h^2 = 1 + \frac{1}{\bar{c}^2}$, $\bar{c} = c/a$.

REFERENCES

1. SMITH,A.M.O. — High Lift Aerodynamics. J.of Air.Vol.12, No.6, pp.5-30 (June 1975).

2. RAY, E.J. and HOLLINGSWORTH,E.G. — Subsonic Characteristics of a Twin-Jet Sweep-Wing Fighter Model with Manoeuvering Devices. N.A.S.A. TN D-6921.

3. GOODMANSON,L.T. and GRATZER,L.B. — Recent Advances in Aerodynamics for Transport Aircraft, Part 1. A.I.A.A. Astro.&Aero., Dec. 1973.

4. JONES,R.T. — Properties of Low Aspect Ratio Pointed Wings at Speeds below and above the Speed of Sound. N.A.C.A. Rep. 835.

5. SMITH J.H.B. — The Properties of a Thin Conically Cambered Wing according to Slender Body Theory. ARC R&M 3135 (1958)

6. HUMMEL, D. — Berechnung der Druckverteilung an Schlanken Flugkorpern mit beliebiger Grundriss-und Querschnittsform in Unter-und Uberschall-stromung, Rep.68/1, Inst.fur Stromungsmechanik, Braunschweig. EOARD,USAF Contract AF 61(052)-933-(1968).

7. COOKE, J.C. — Properties of a Two-Parameter Family of Thin Conically Cambered Delta Wings by Slender Body Theory. ARC R & M 3249 (1960).

8. BROWN, C.E. and MICHAEL, W.H.Jr. — On Slender Wings with Leading Edge Separation. NACA TN 3430 (1954).

9. SQUIRE, L.C. — Camber Effects on the Non-Linear Lift of Slender Wings and Sharp Leading Edges. ARC 27651, January 1966.

10. JOBE, C.E. — An Aerodynamic Theory of Slender Wings with Leading Edge Separation. Unpublished M.Sc. Thesis, Ohio State Univ. 1966.

11. LOWSON, M.V. — The Separated Flows on Slender Wings in Unsteady Motion. ARC R & M 3448 (1963).

12. SMITH, J.H.B. — A Theory of the Separated Flow from the Curved Leading Edge of a Slender Wing. ARC R & M 3116 (1957).

13. SMITH, J.H.B. — Improved Calculations of Leading Edge Separation from Slender Thin Delta Wings. Roy.Soc.Proc.Series 306, 30 July 1968, pp.67-90.

14. BARSBY, J.E. — Flow Past Conically-Cambered Slender Delta Wings with Leading Edge Separation. ARC R & M 3748 (1972).

15. LEVINSKY, E.S. and WEI, M.H.Y. — Non-linear Lift and Pressure Distribution on Slender Conical Bodies with Strakes at Low Speeds. NASA CR-1202 (1968).

16. FERNANDEX, J. and HOLLA, V.S. — Spanwise Cambered Delta Wing with Leading Edge Separation. A.I.A.A. J.of Aircraft, Vol.14,No.3,pp.276-82, March 1977.

17. WEBER, J. — The Calculation of the Pressure Distribution on Thick Wings of Small Aspect Ratio at Zero Lift in Subsonic Flow. ARC R & M No.2993, 1957.

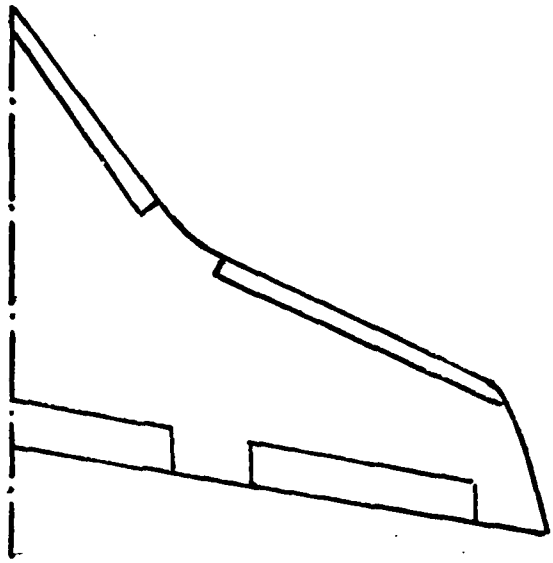

(b) HIGHLY SWEPT APEX

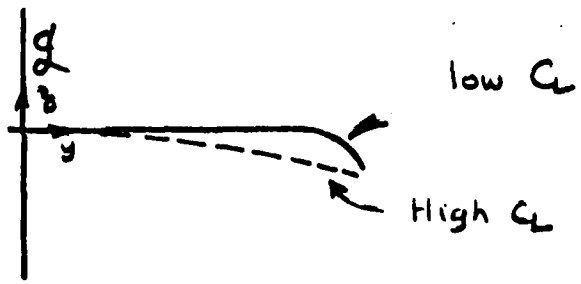

(c) CAMBER SHAPES

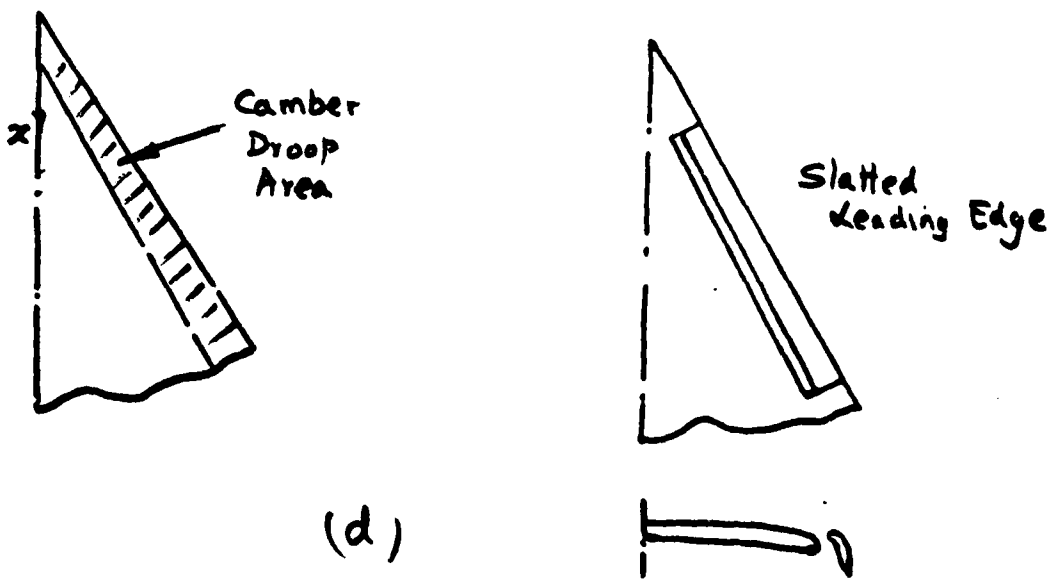

(d)

FIG. 1.

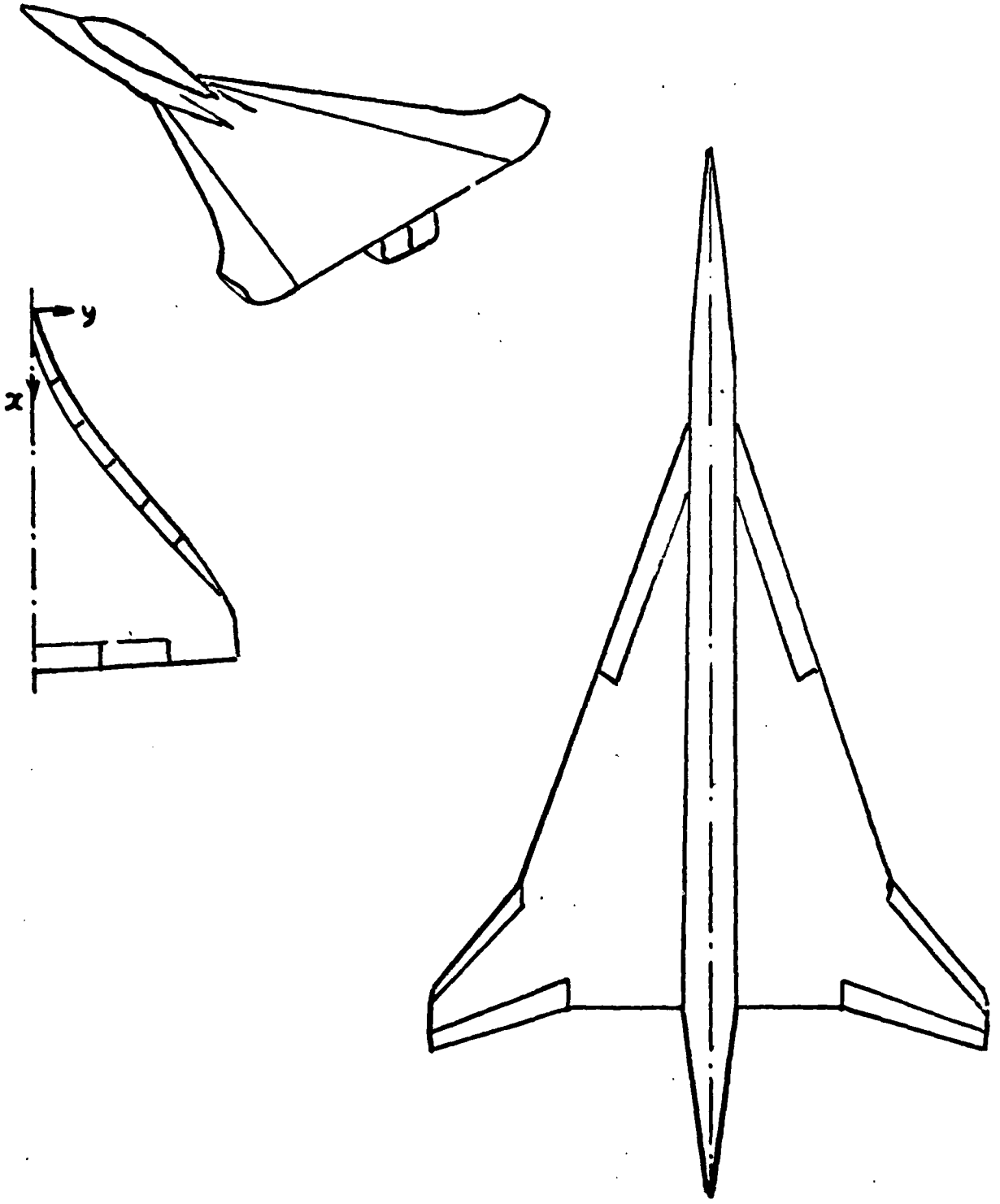

(a) HIGHLY SWEPT BACK WINGS

FIG 1

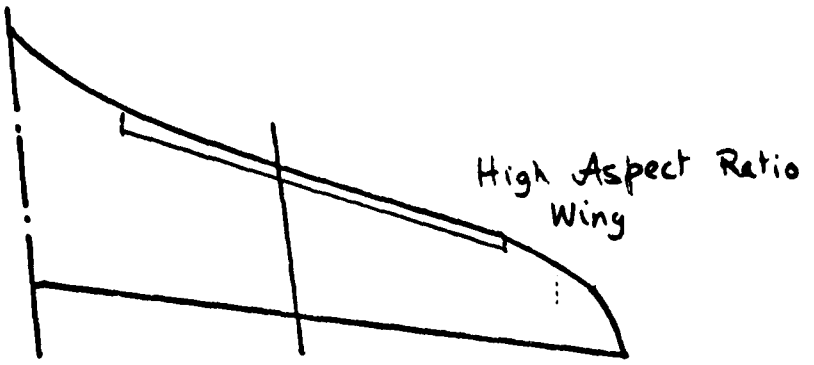

FIG. 2. 'CONVENTIONAL' AIRCRAFT WING

FIG. 3. 2-D AEROFOIL METHODS

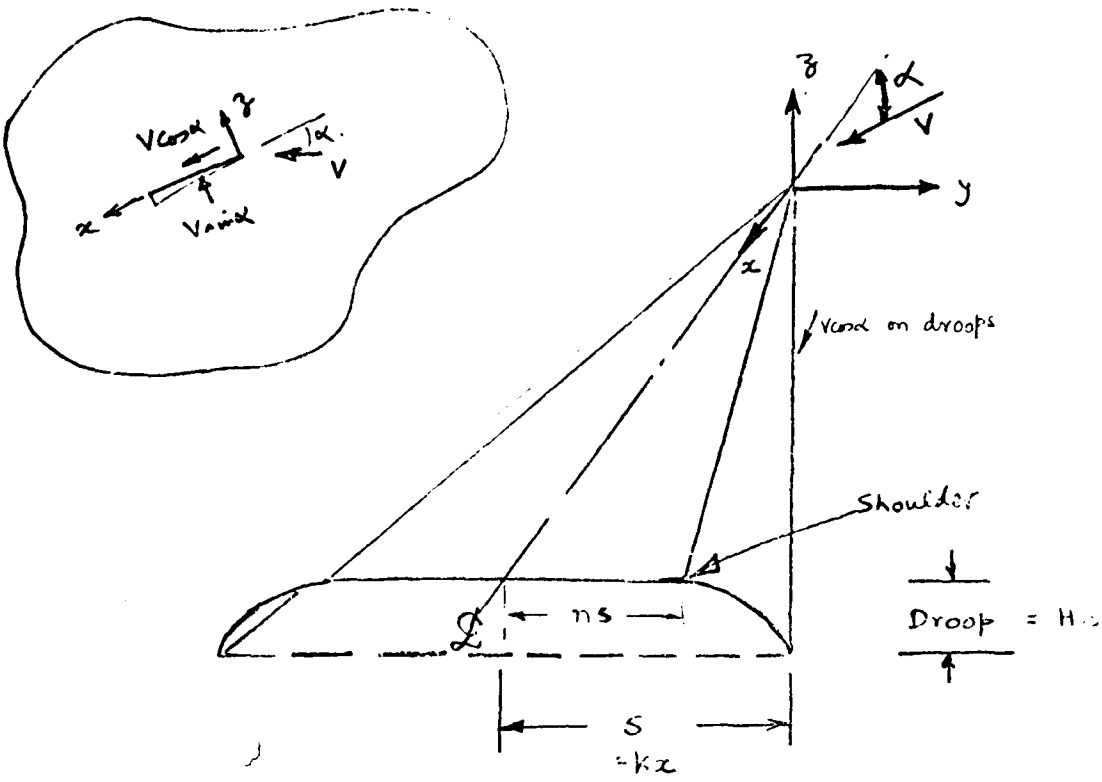

WING GEOMETRY

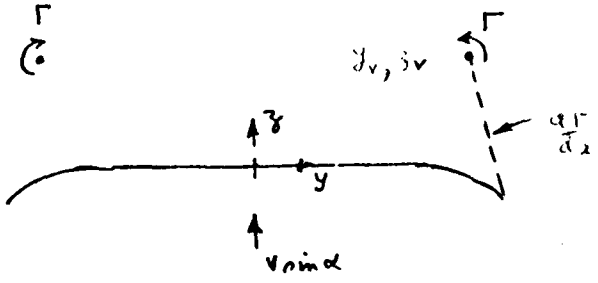

CROSS-FLOW PLANE

(with Primary Vortices)

FIG. 4. MODEL

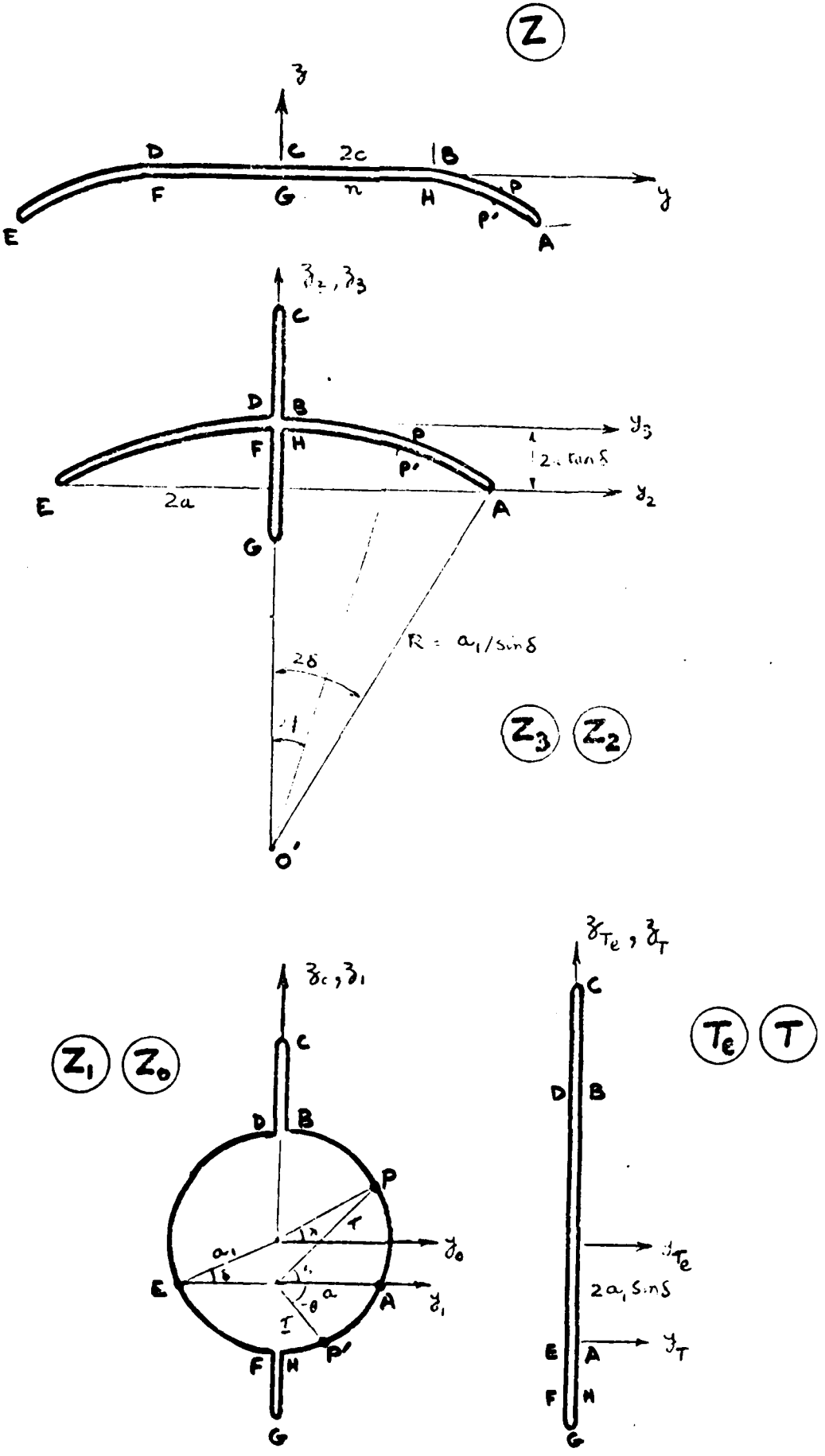

FIG. 5. CONFORMAL TRANSFORMATIONS

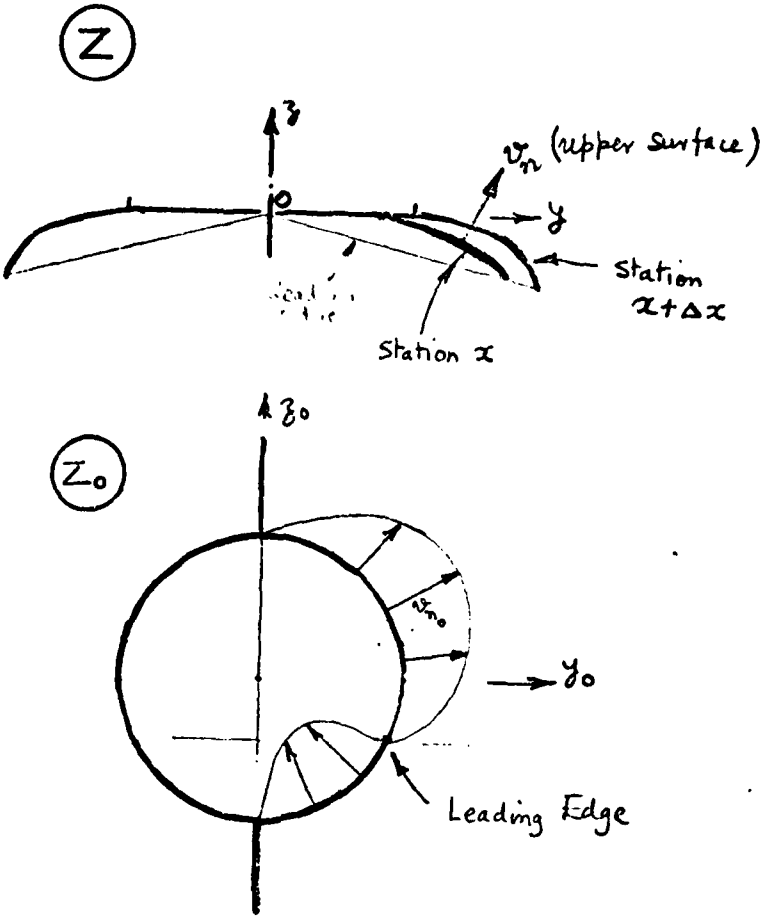

FIG. 6. NORMAL VELOCITY ON DROOPS

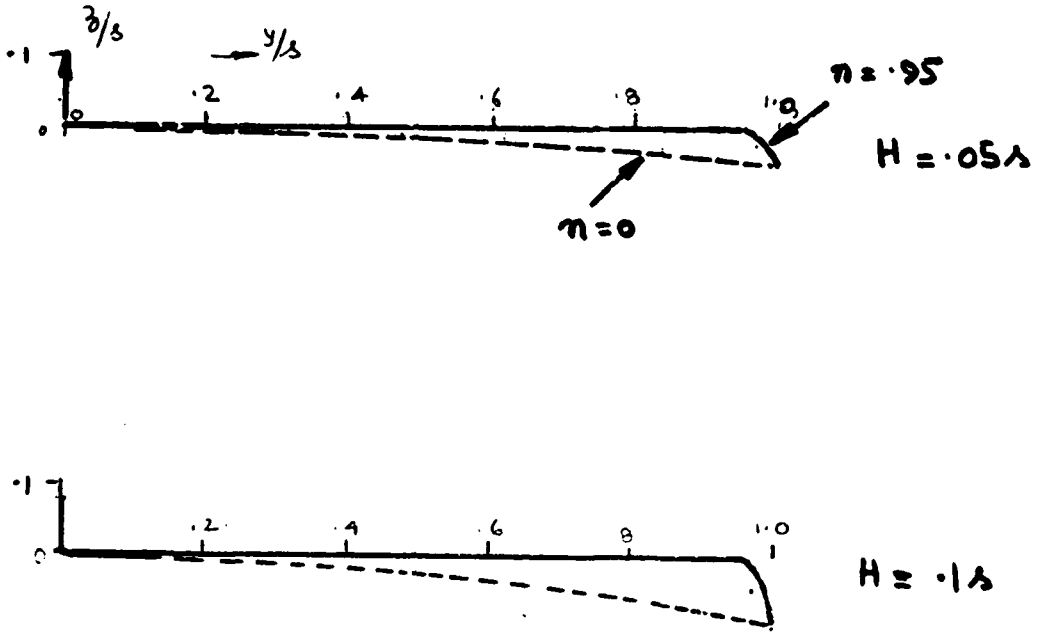

FIG. 7. CAMBER LINES

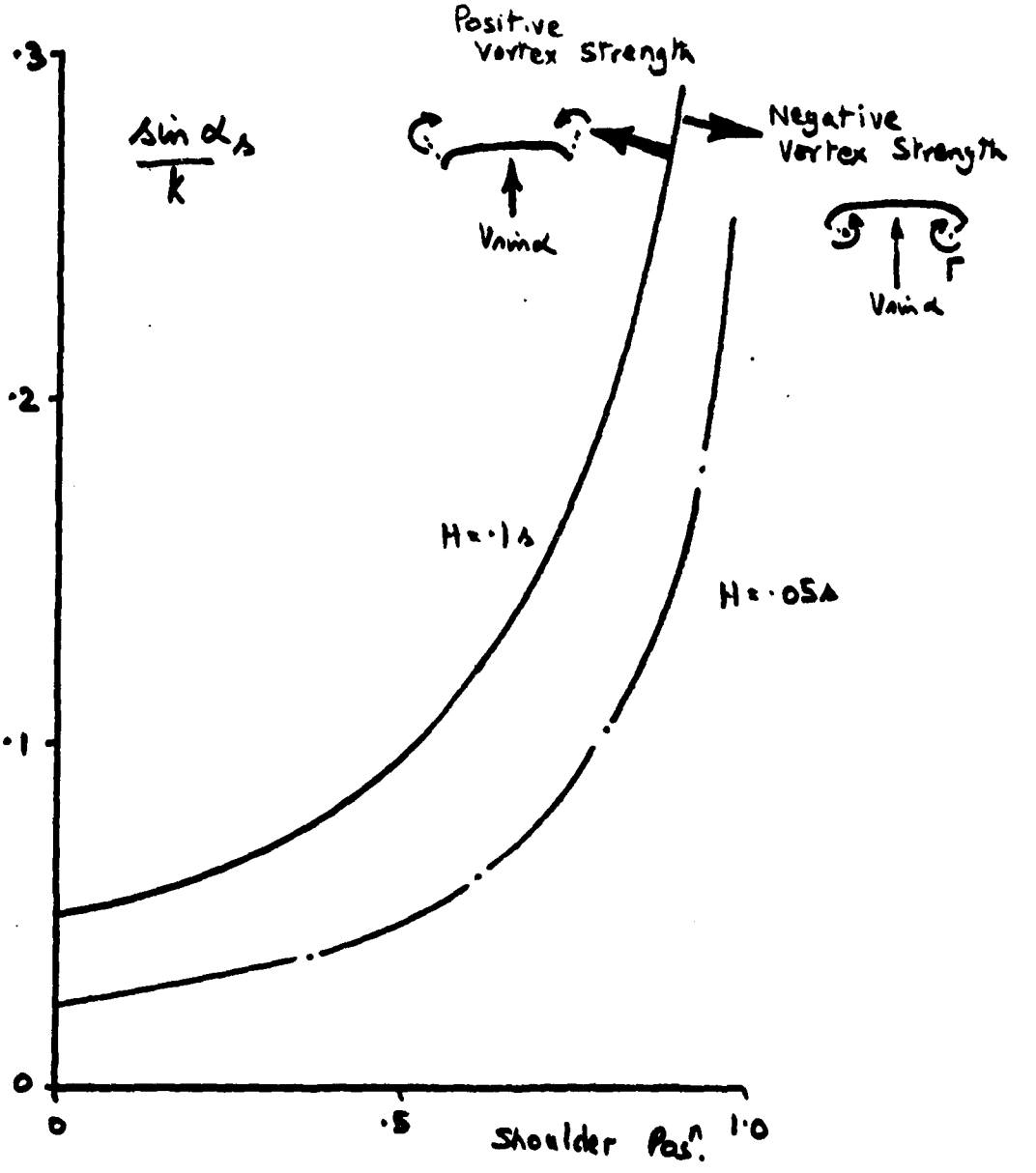

FIG. 8. VARIATION OF $\sin\alpha_s/k$ ~ SHOULDER POSN

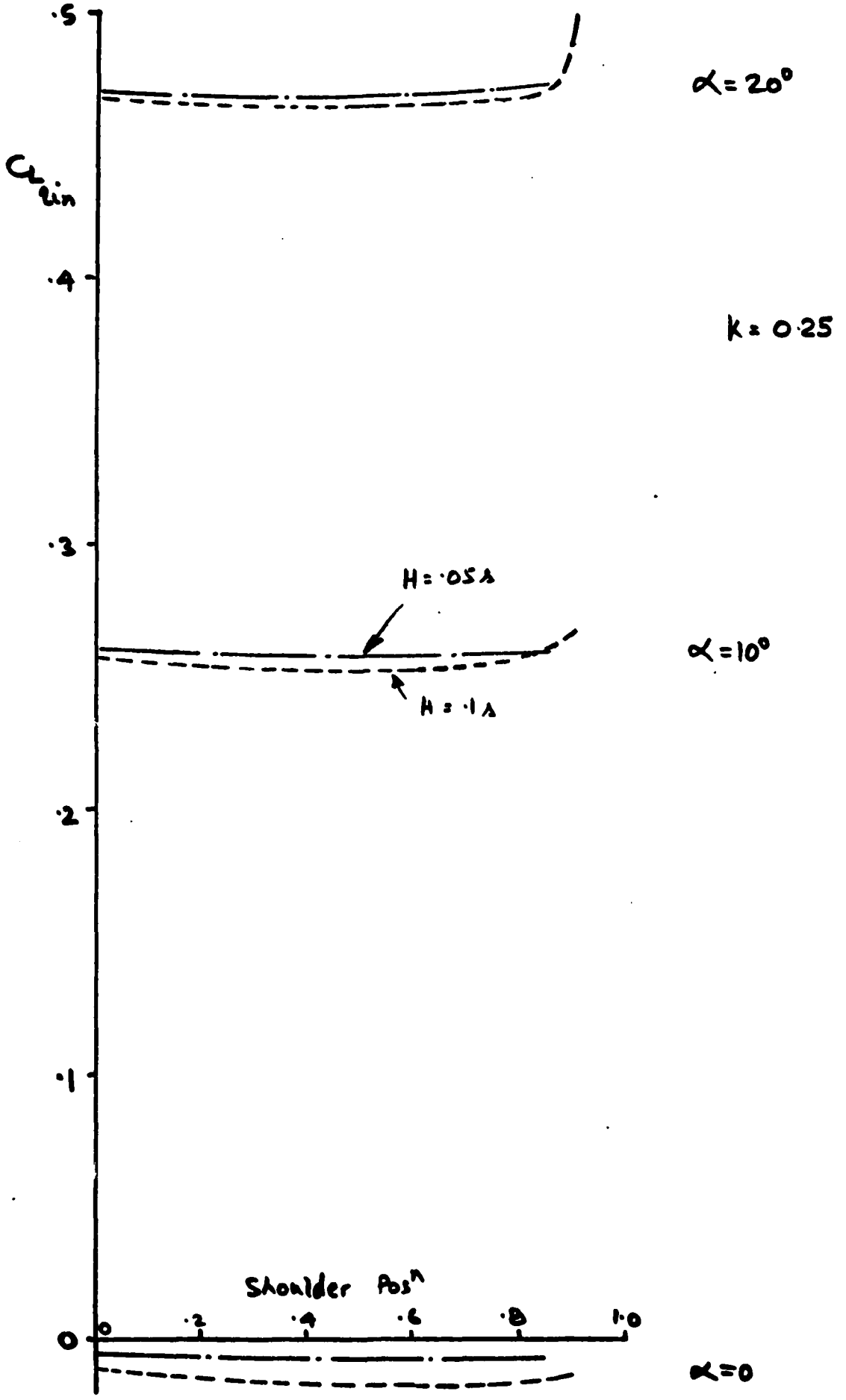

FIG. 9. EFFECT OF SHOULDER POS^N ON ATTACHED FLOW LIFT

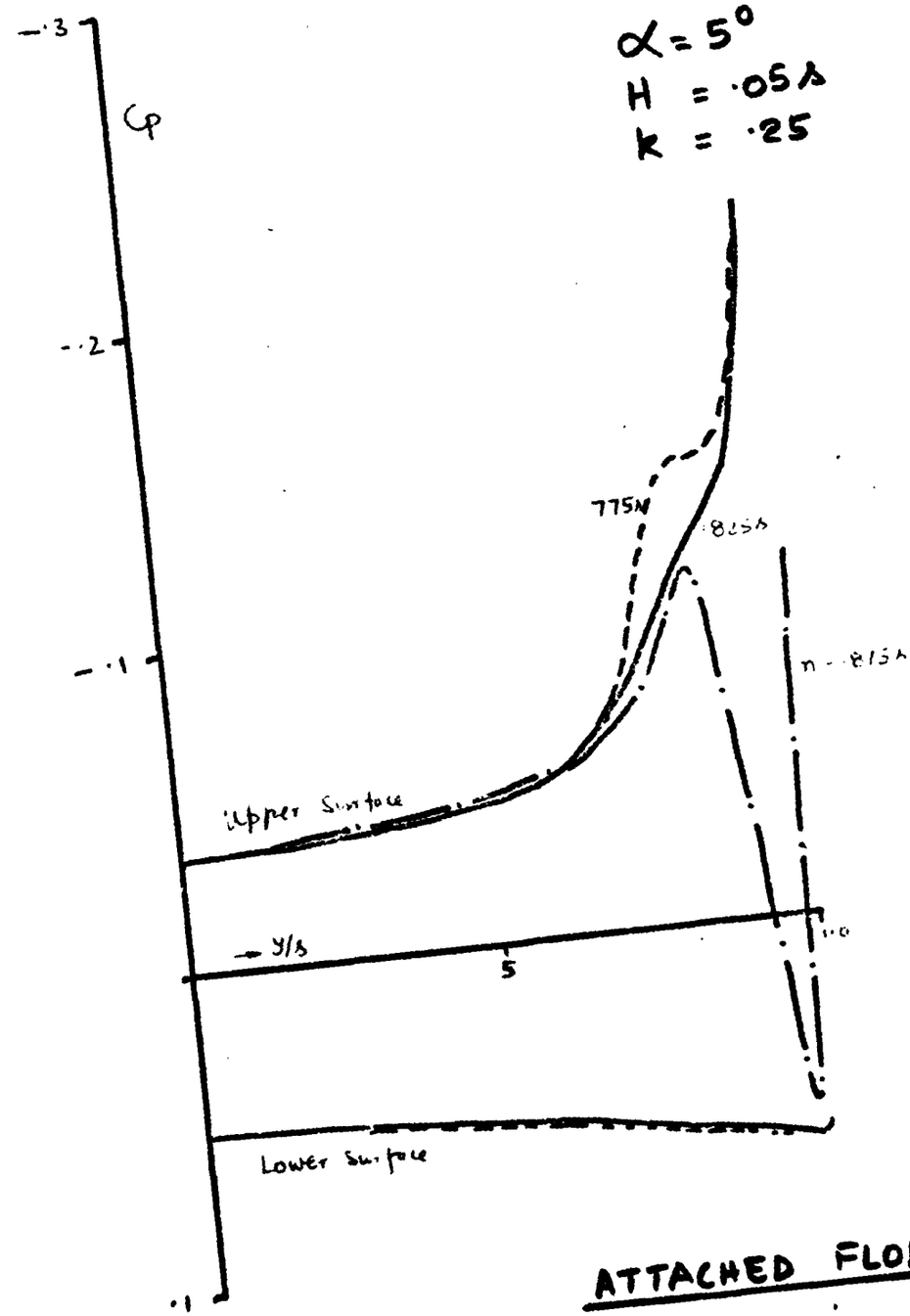

ATTACHED FLOW

FIG. 10. EFFECT OF SHOULDER POSN. ON Cp DISTRIBUTION

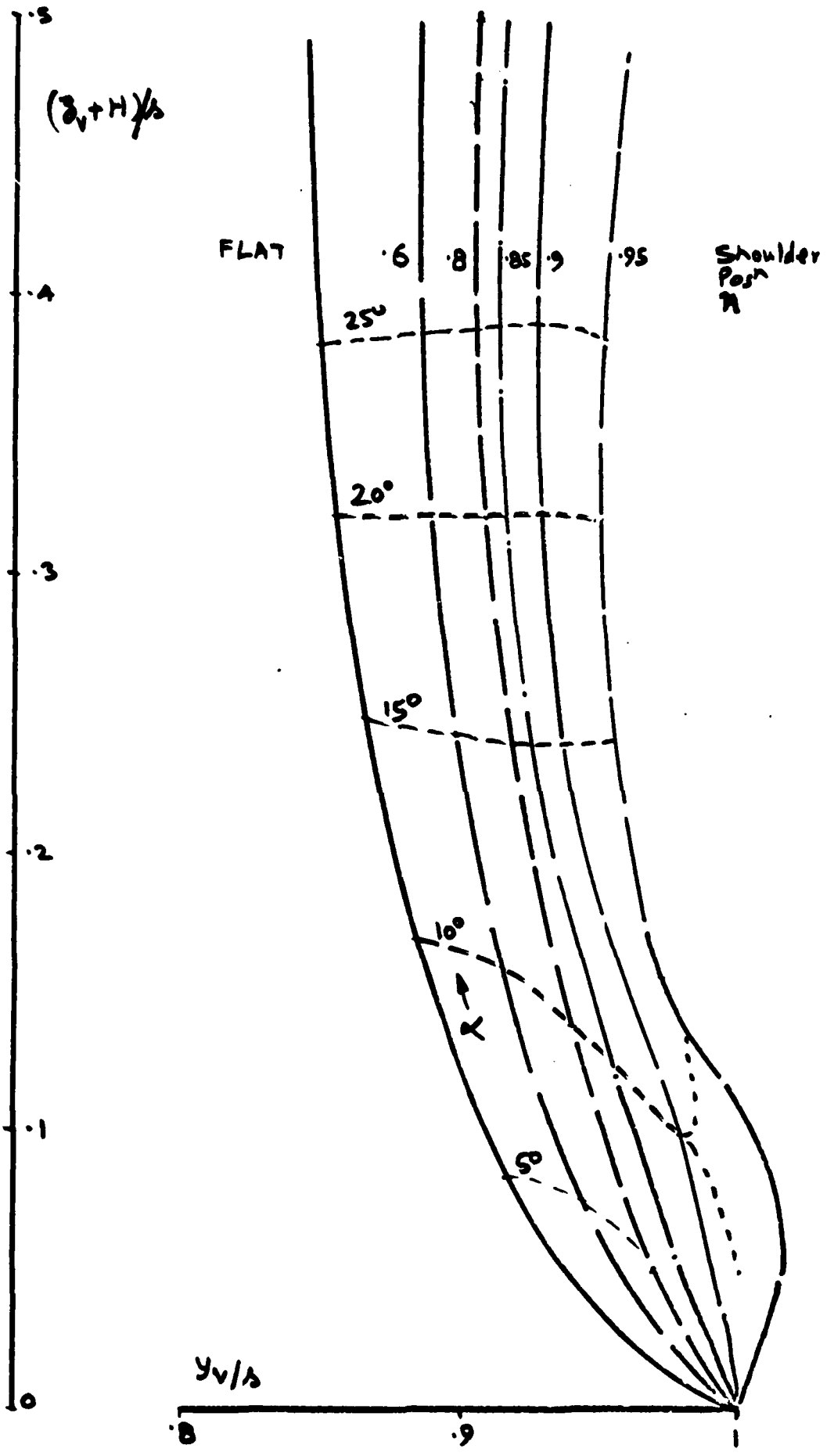

(i) VORTEX LOCUS

FIG. 11 H = ·05s WING, k = 0·25

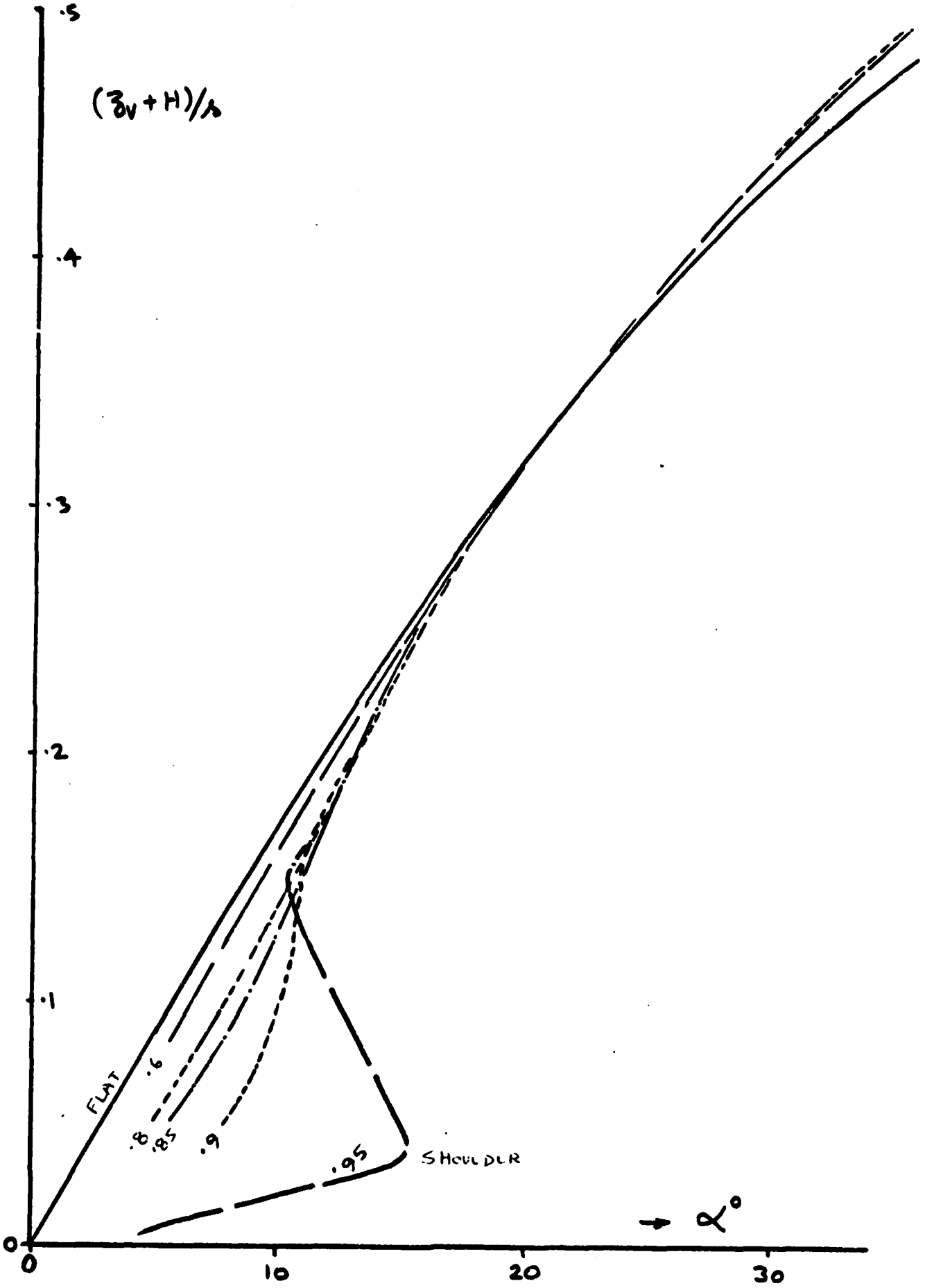

(ii) Vortex Height ~ α

FIG. 11. H = ·05 s WING.

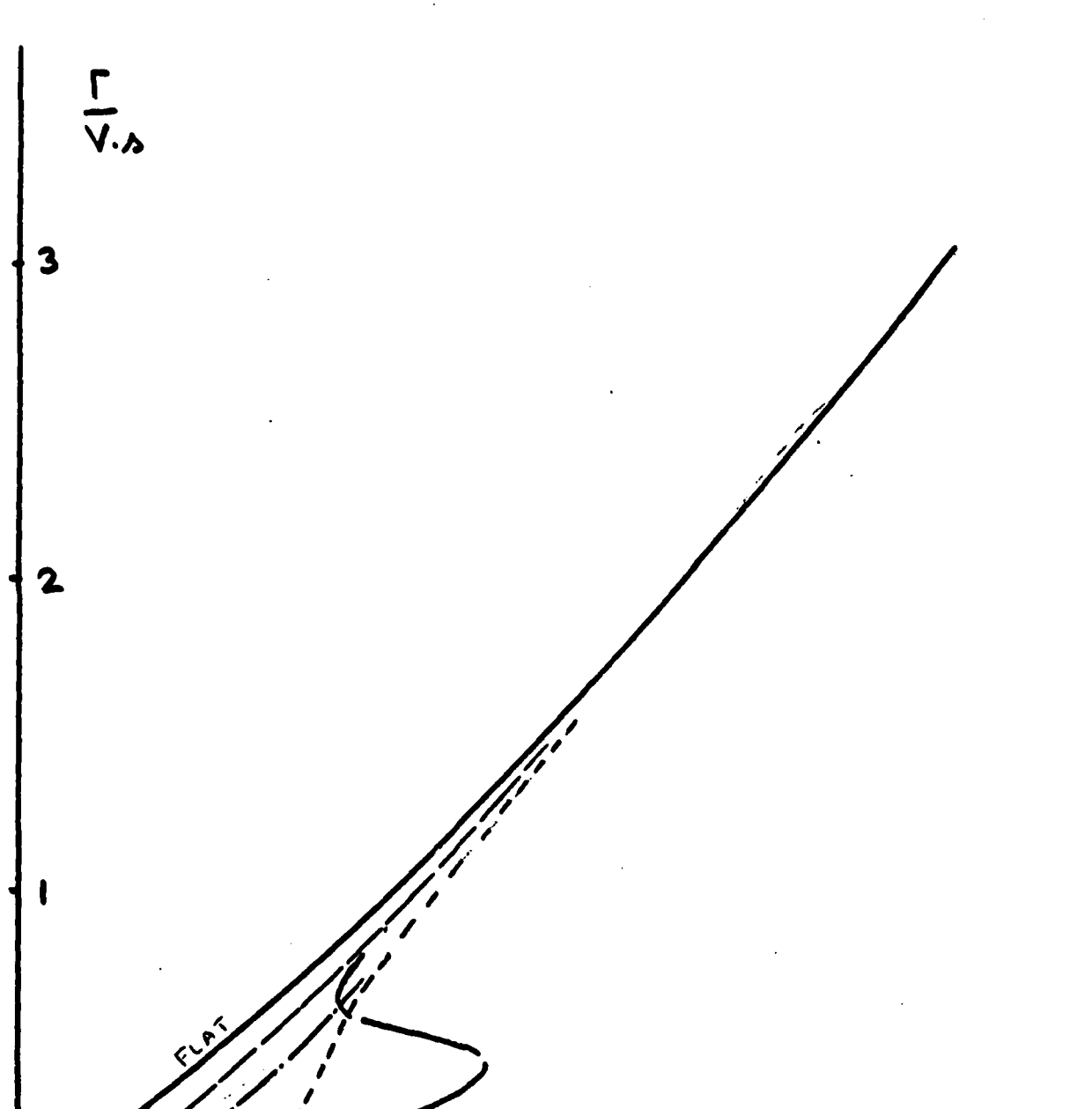

(iii) Vortex Strength $\sim \alpha$

FIG. 11. H = .05s WING.

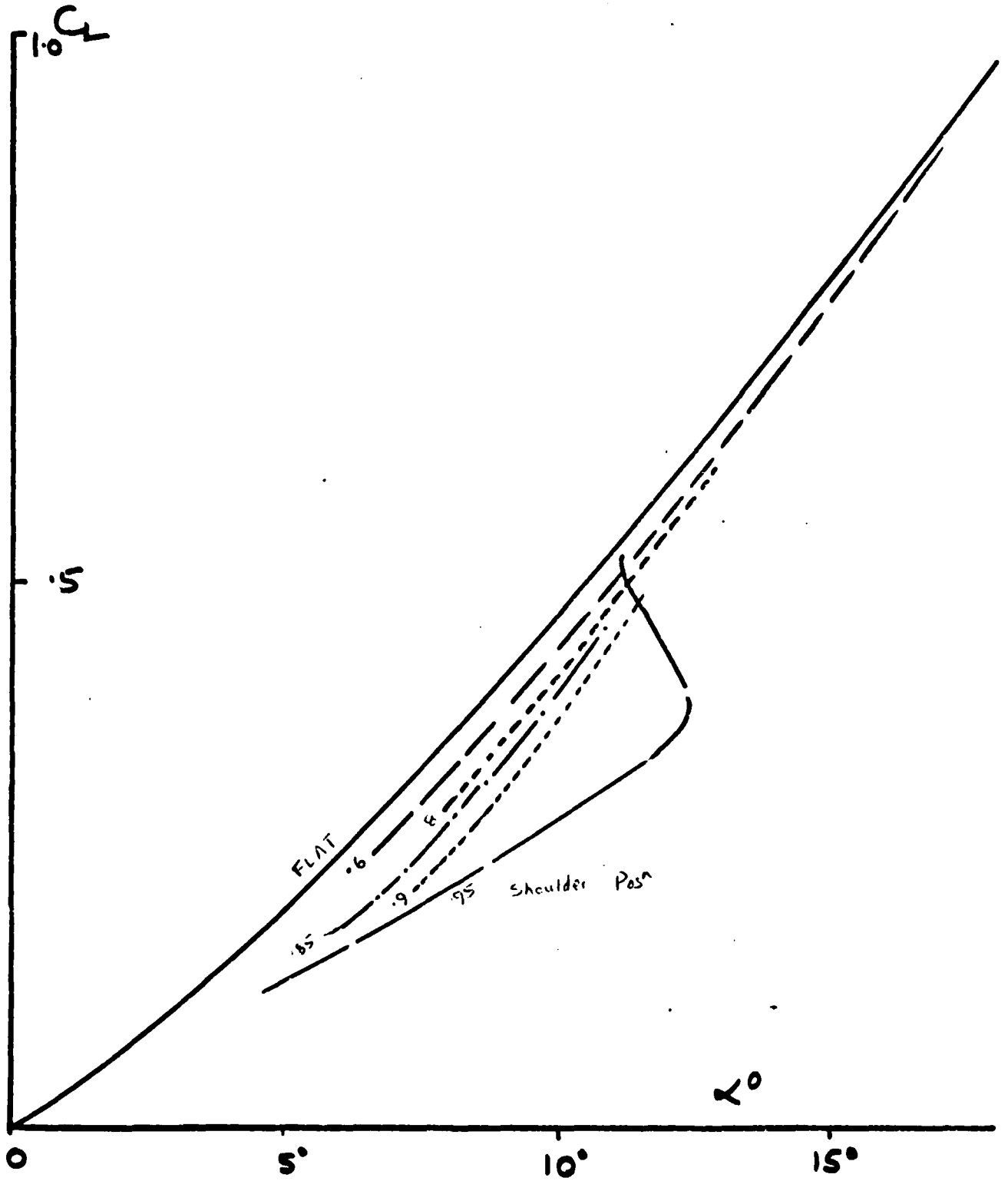

(iv) $C_L \sim \alpha$

FIG. 11. H = ·05 Λ WING

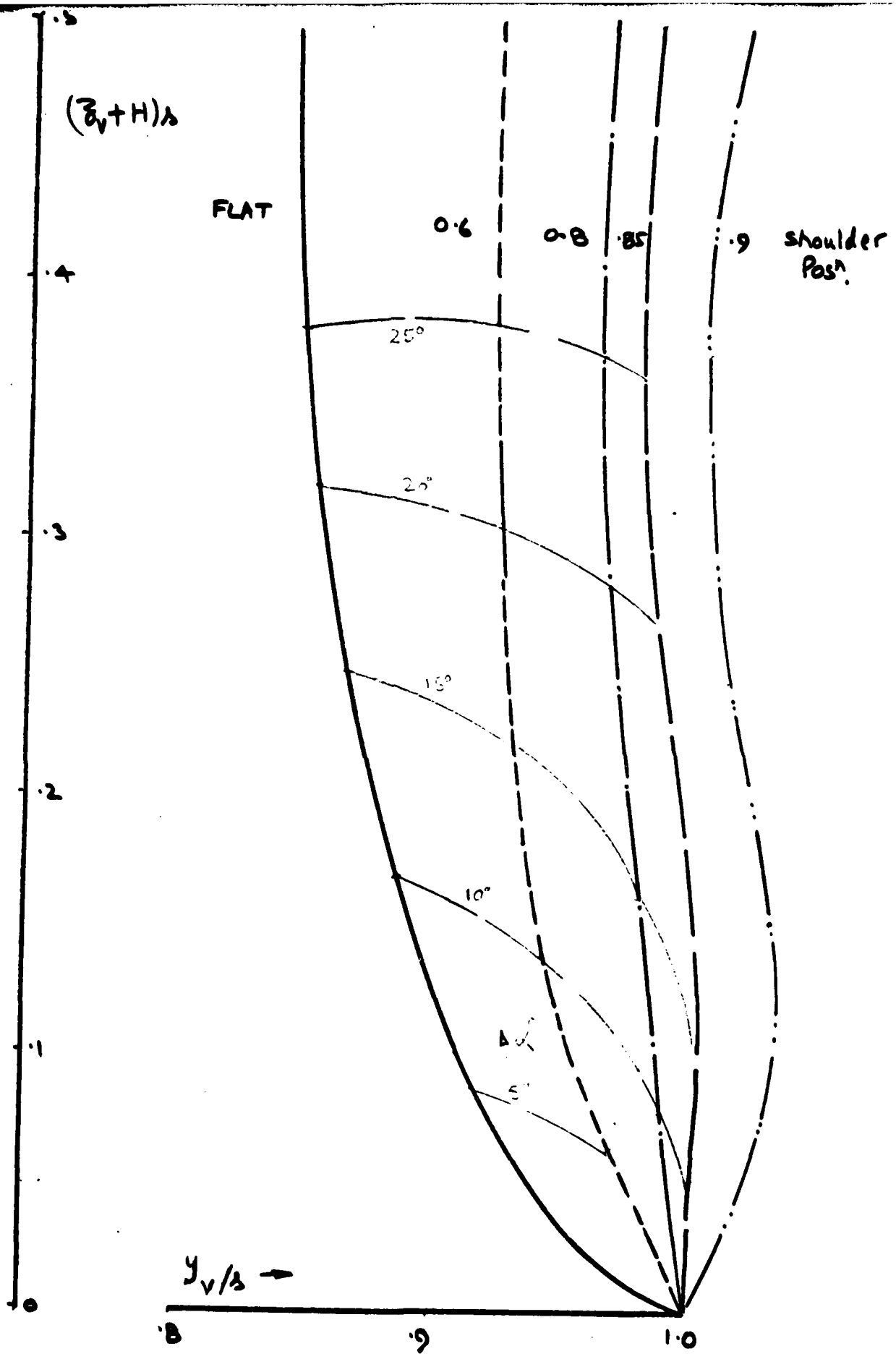

(i) VORTEX LOCUS

FIG. 12. H = ·10 WING, k = 0·25

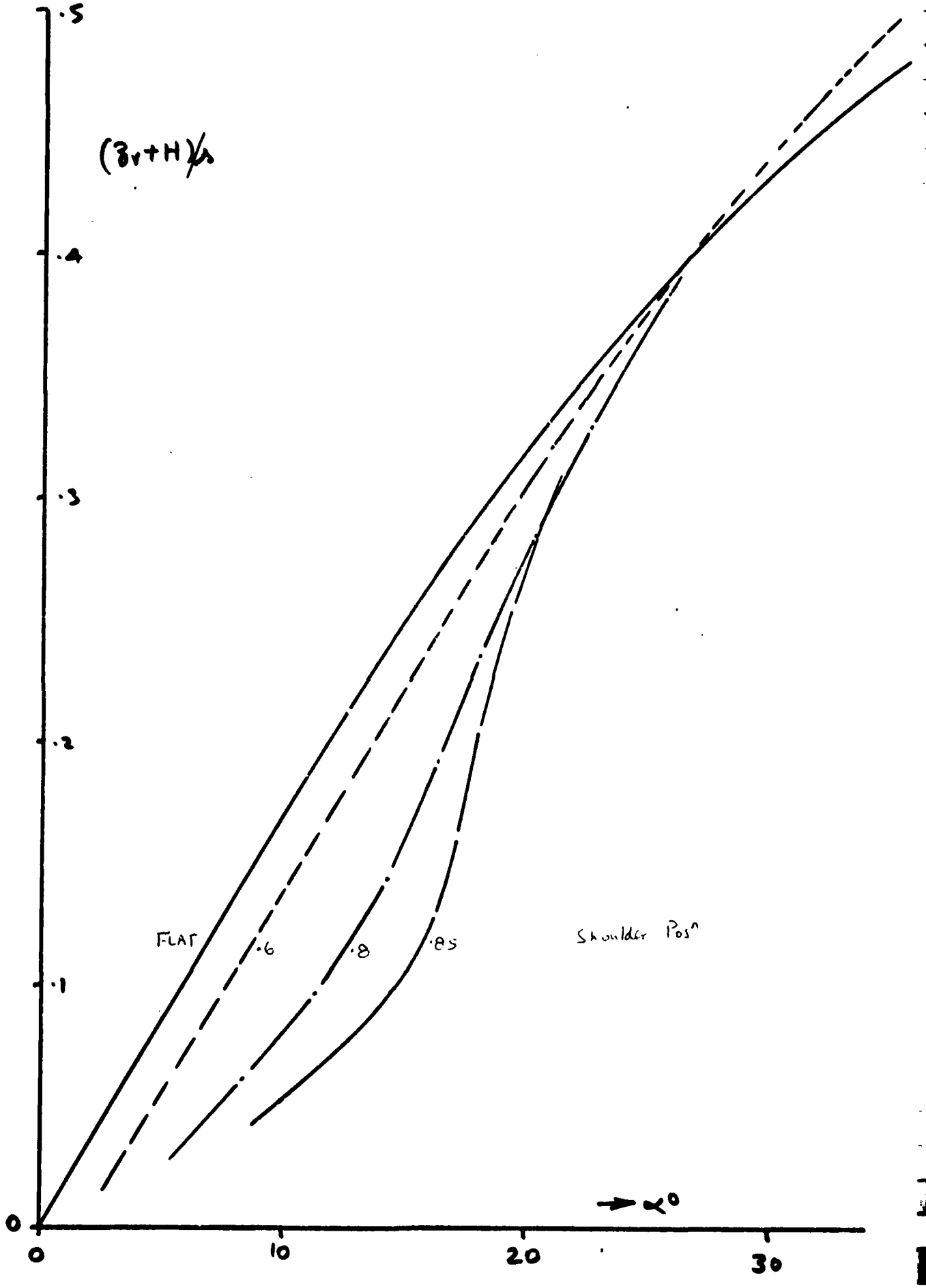

(ii) vortex Height ~α

FIG. 12. H = ·10 WING

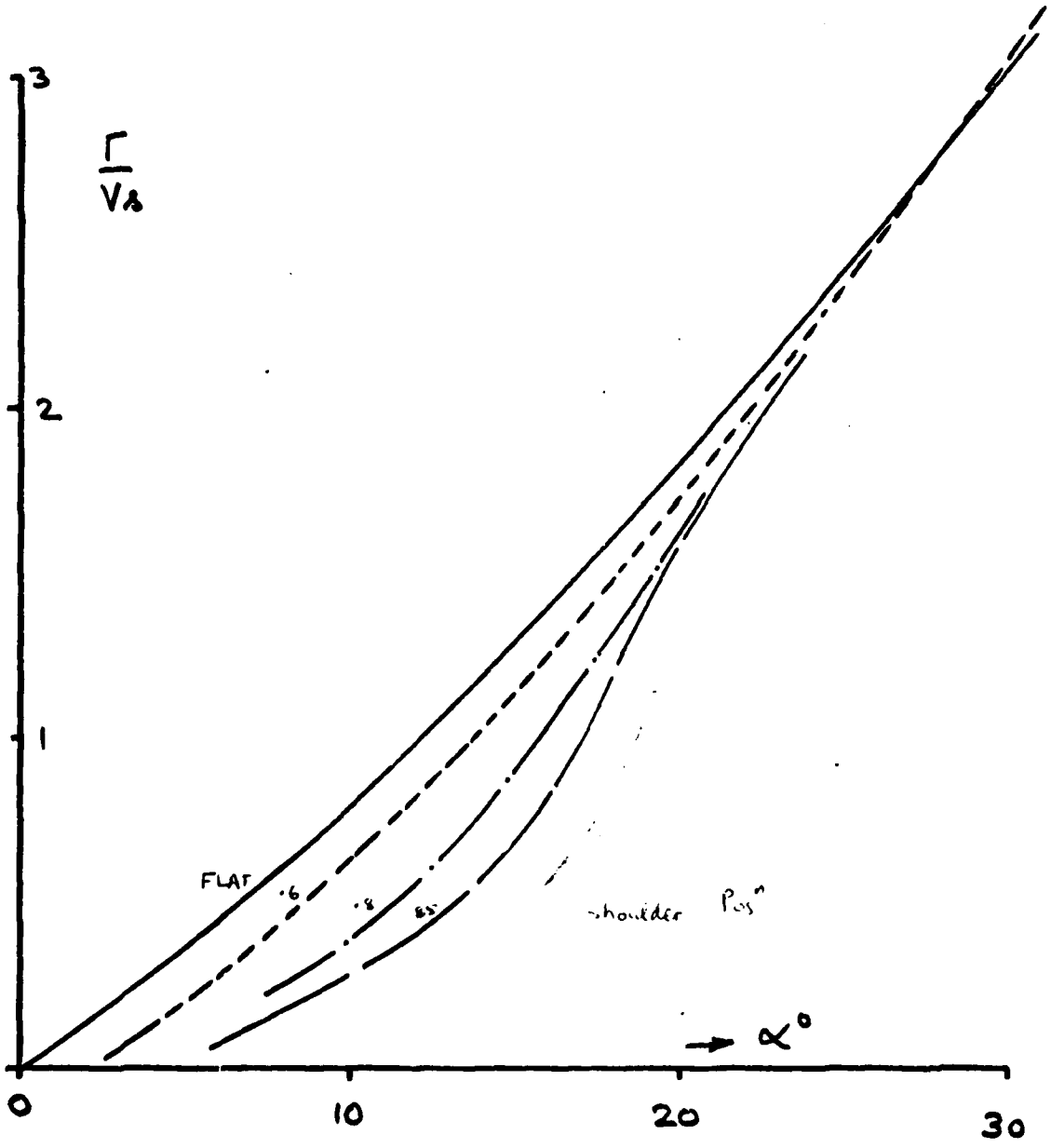

(iii) Vortex Strength ~ α

FIG. 12. H = ·10 WING

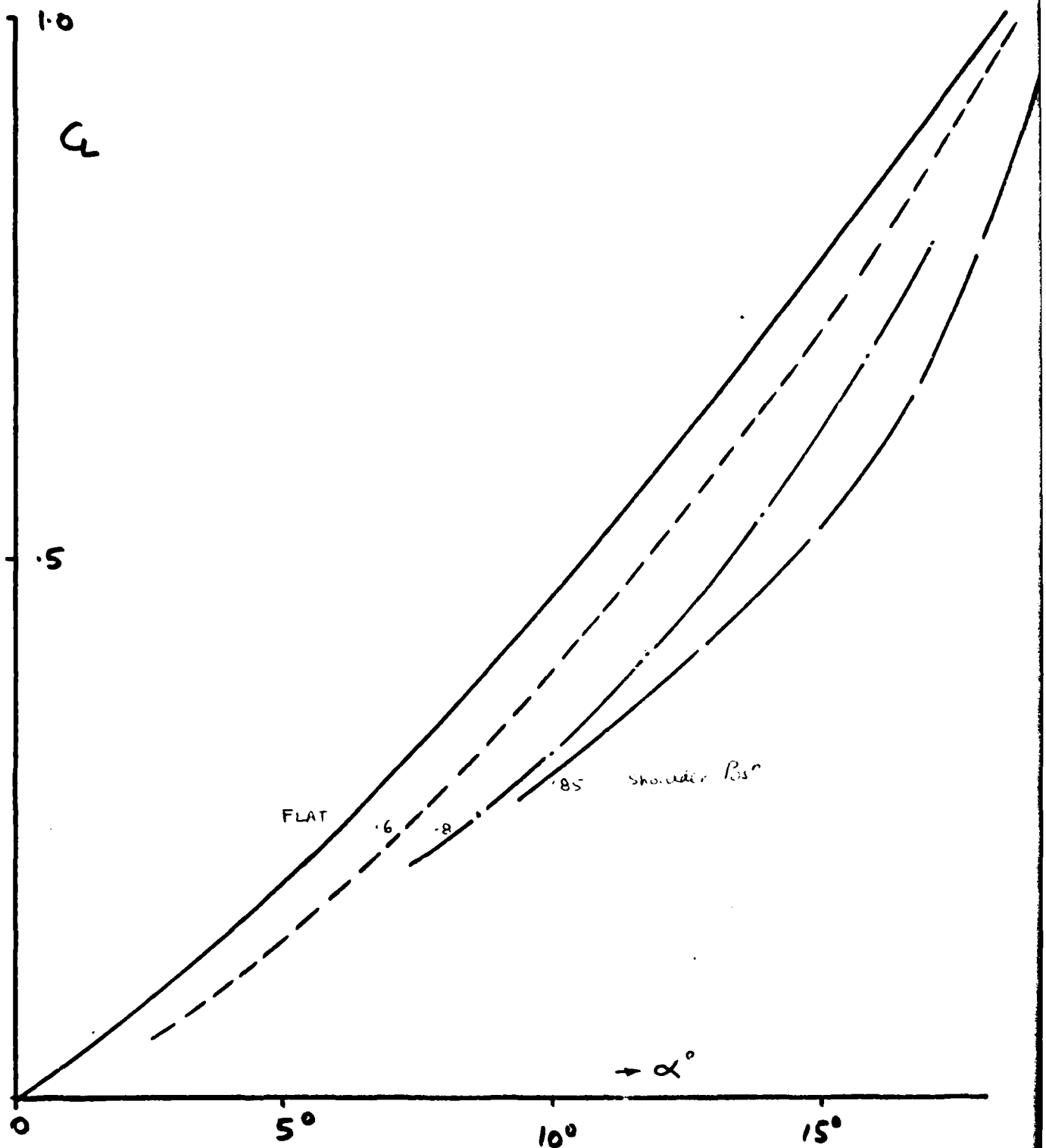

(iv) $C_L \sim \alpha$

FIG. 12. H = ·10 WING

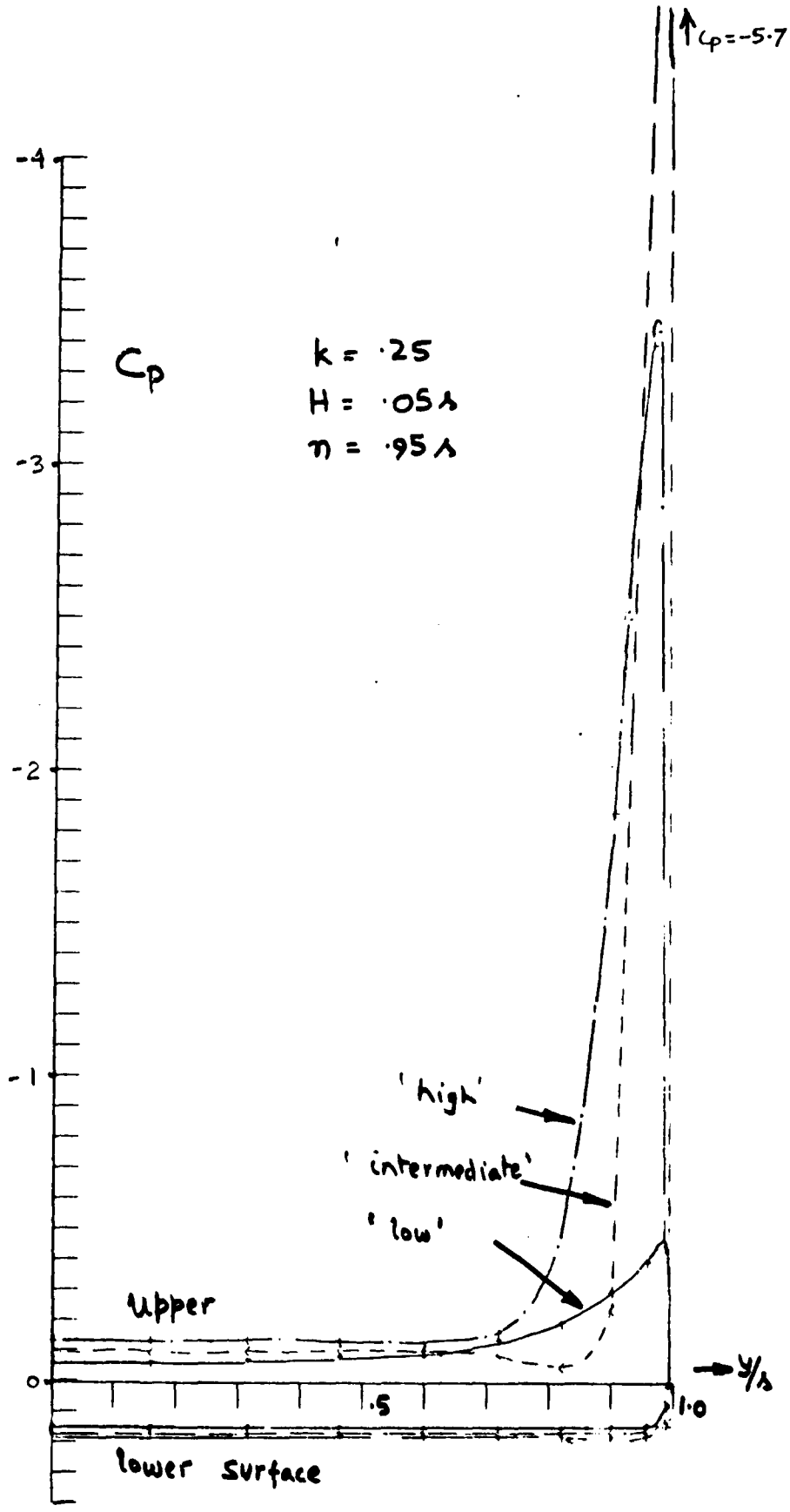

FIG. 13. Pressure Distributions at $\alpha = 11.7°$ for 3 vortex Positions.

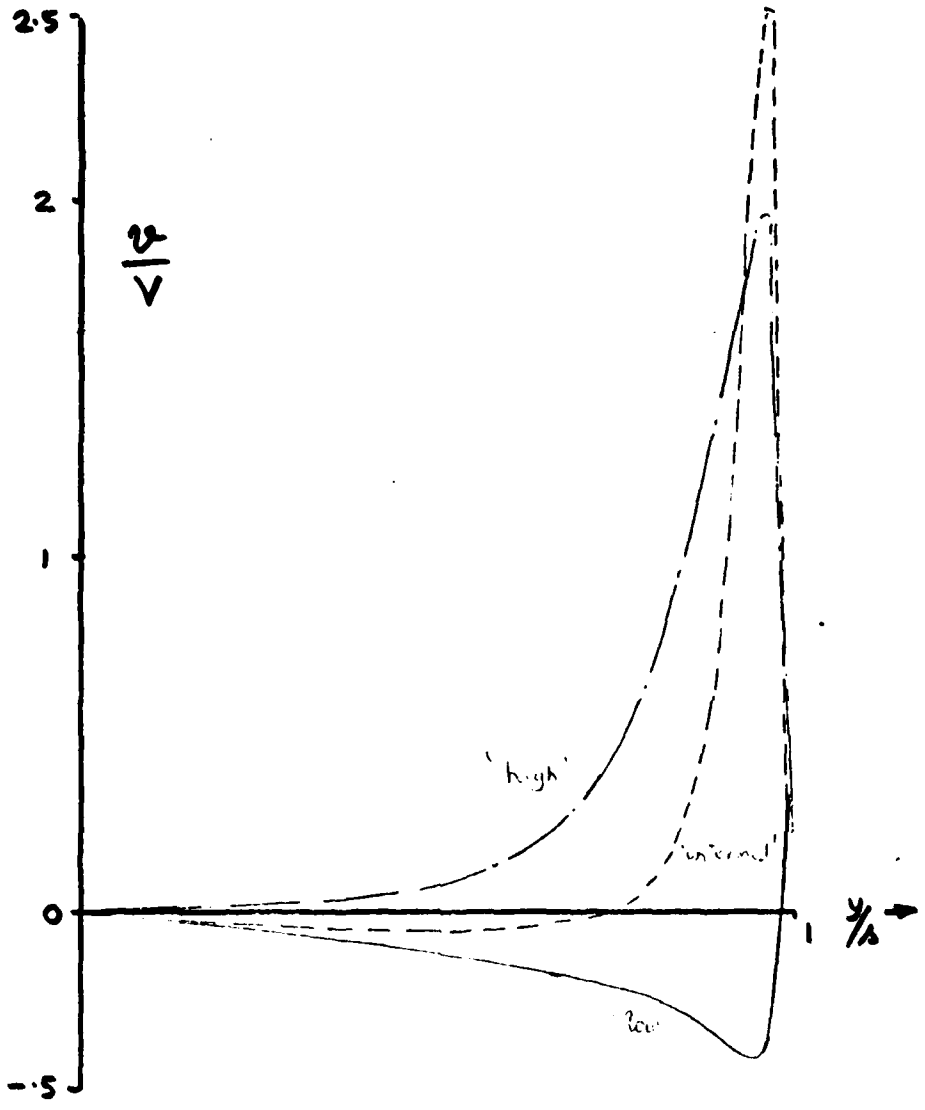

FIG. 14. Variation of spanwise Velocity Tangential to Upper Surface for 3 Vortex Pos^ns.

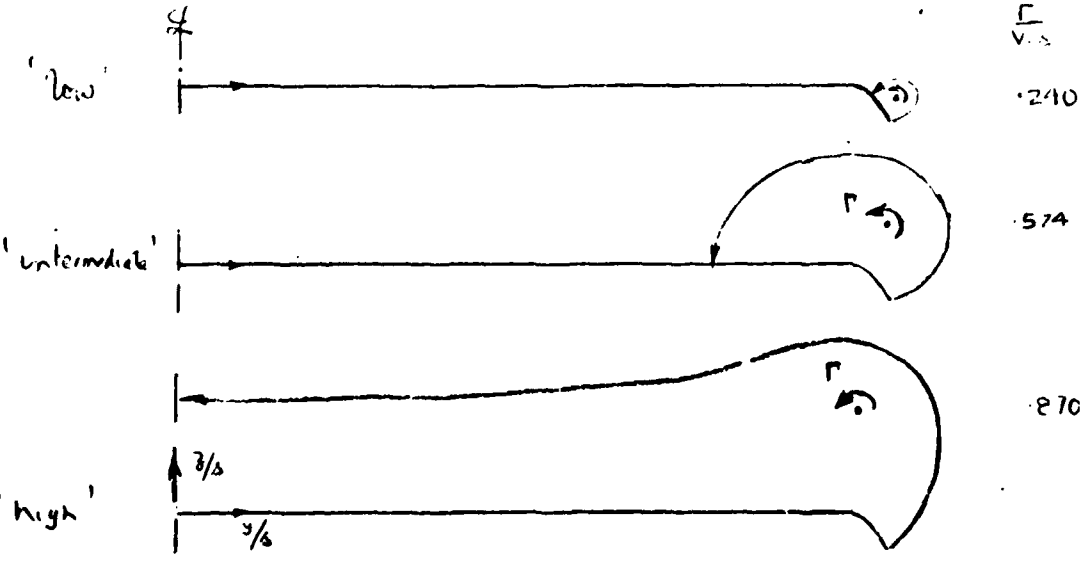

FIG. 15. POSSIBLE RE-ATTACHMENT STREAMLINES FOR 3 VORTEX POS^NS

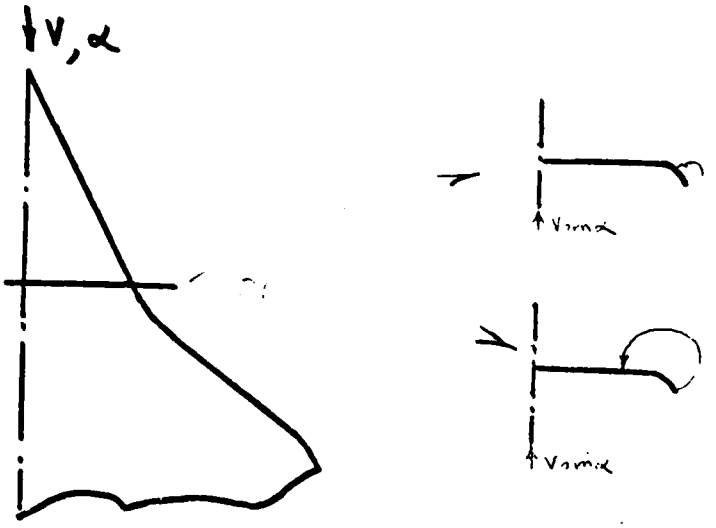

(a) L.E. Sweepback Decreasing aft

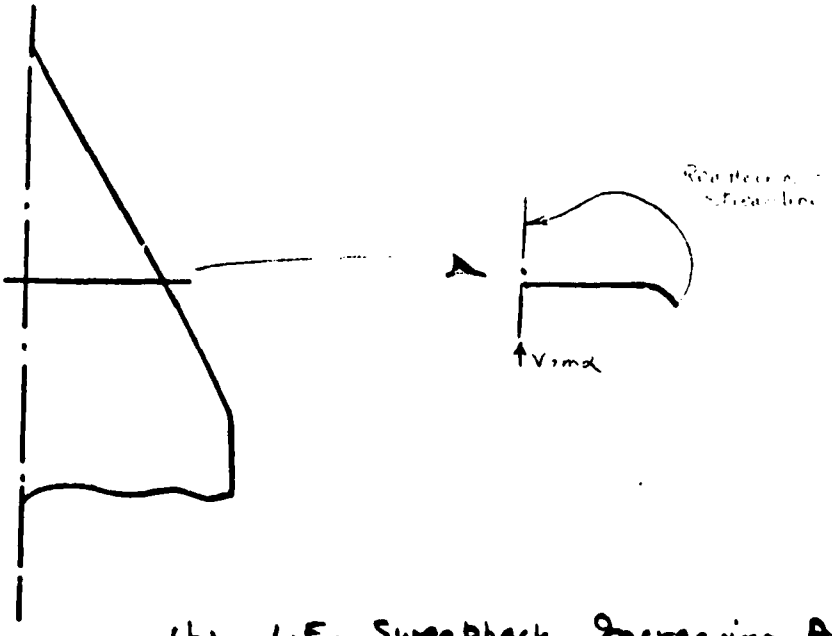

(b) L.E. Sweepback Increasing Aft.

FIG. 16. POSSIBLE EFFECT OF PLANFORM SHAPE

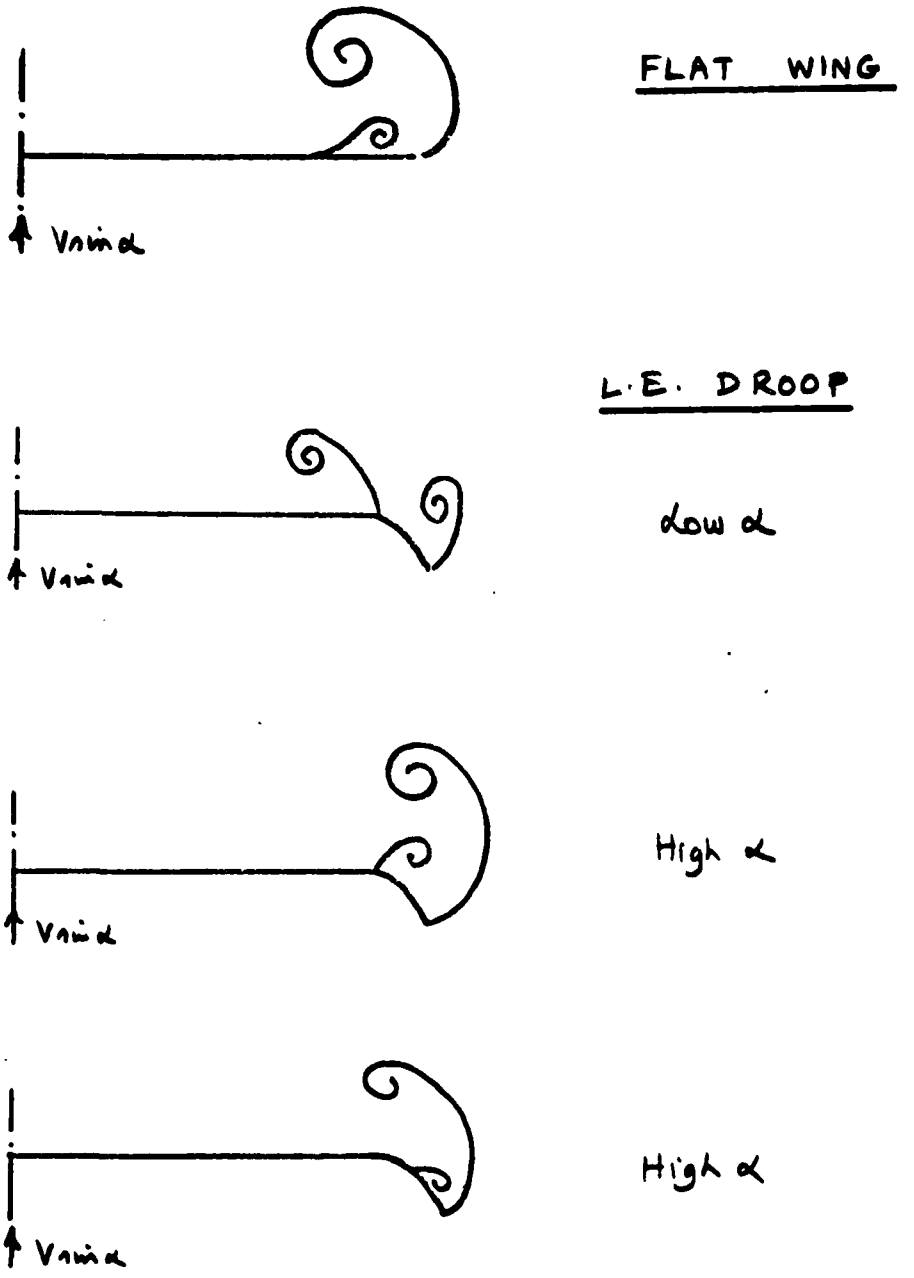

FIG. 17. MULTIPLE VORTEX SYSTEMS

Lovinsky & Wei

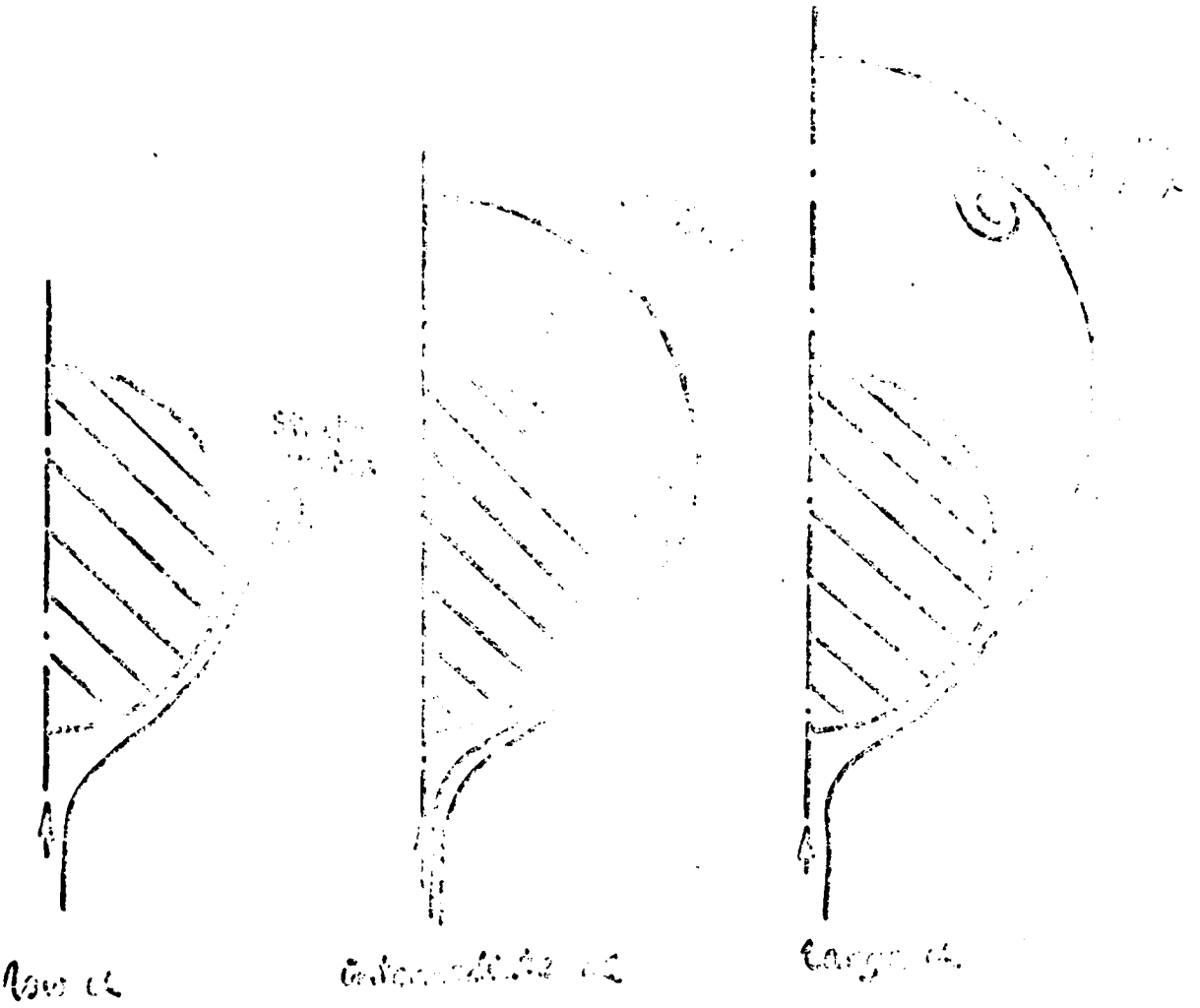

FIG. 18 Multiple vortex systems on Conical Bodies with strakes.

k = ·25
H = ·05 λ

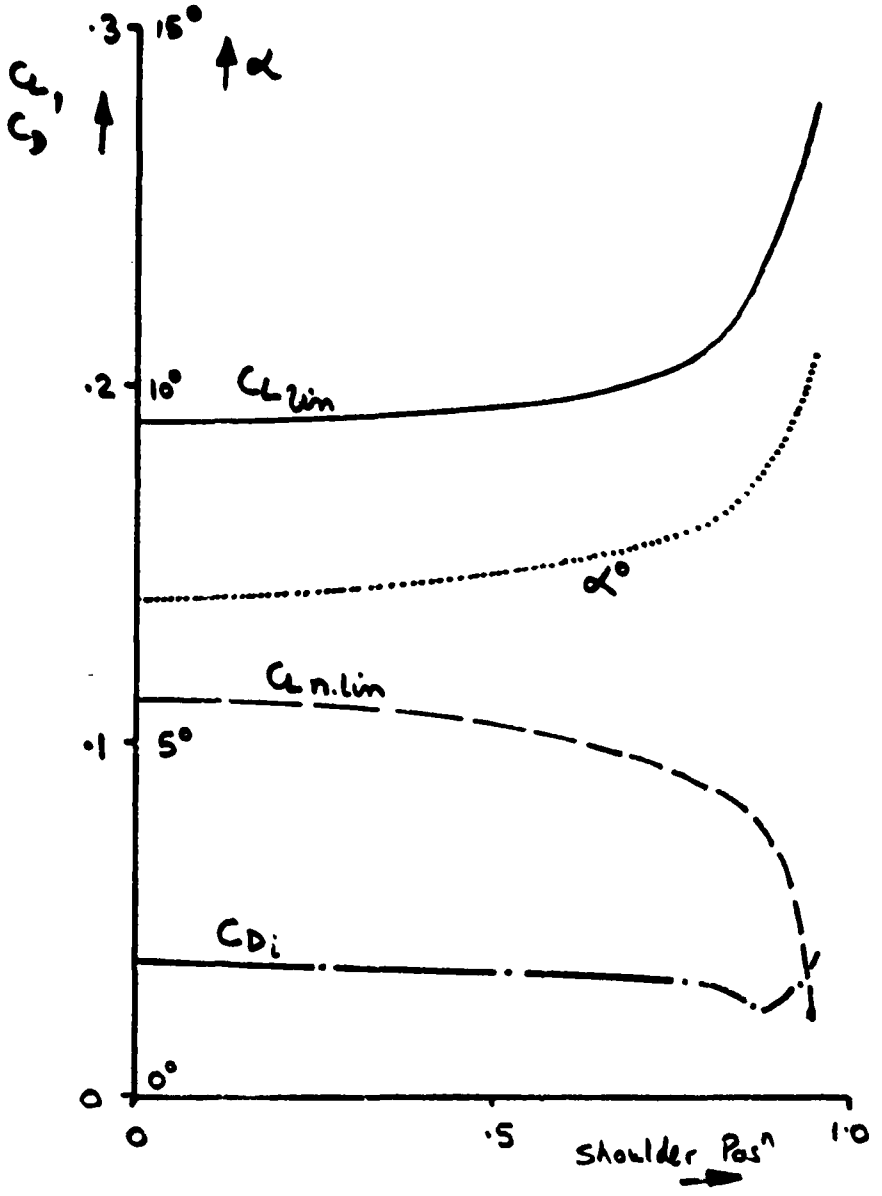

FIG. 19. EFFECT OF VARYING SHOULDER POSITION OF CAMBER AT FIXED $C_L = 0·3$

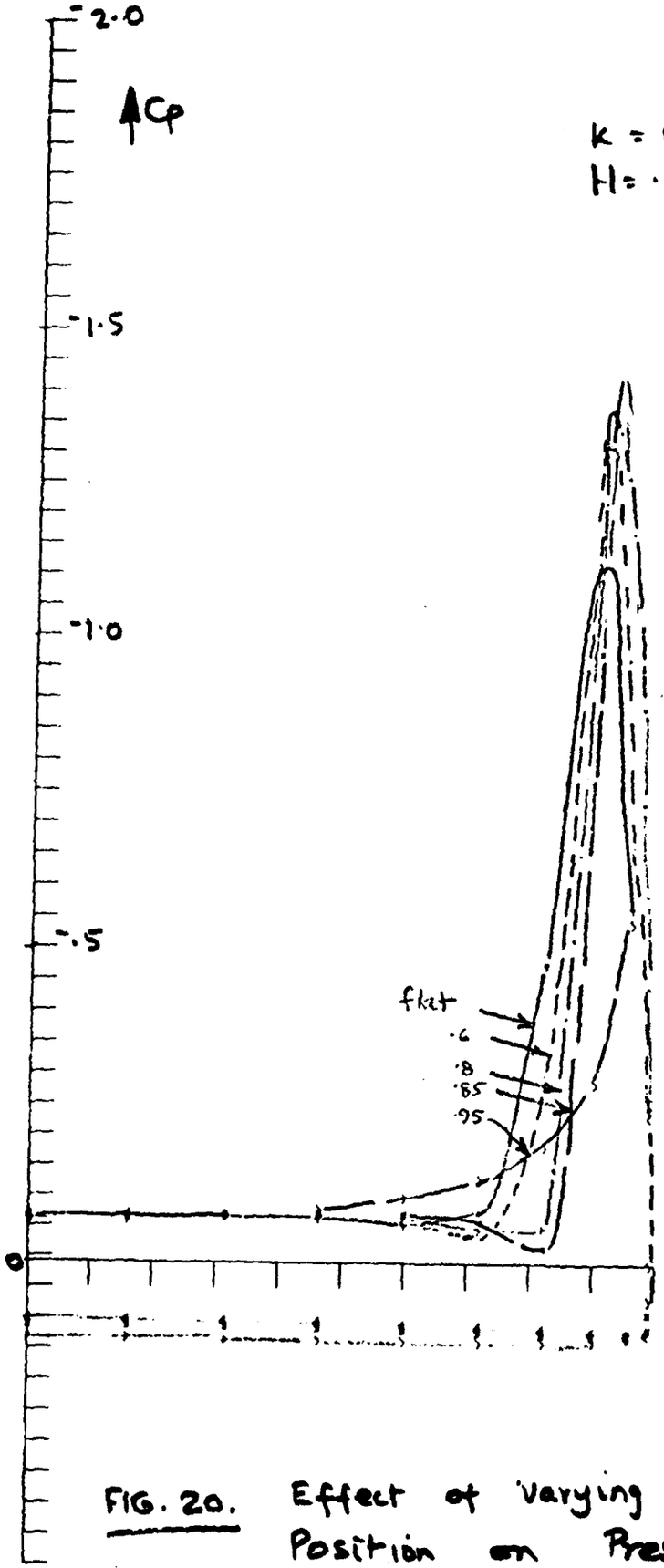

FIG. 20. Effect of varying Shoulder Position on Pressure Distribution at Constant $C_L = 0.3$.

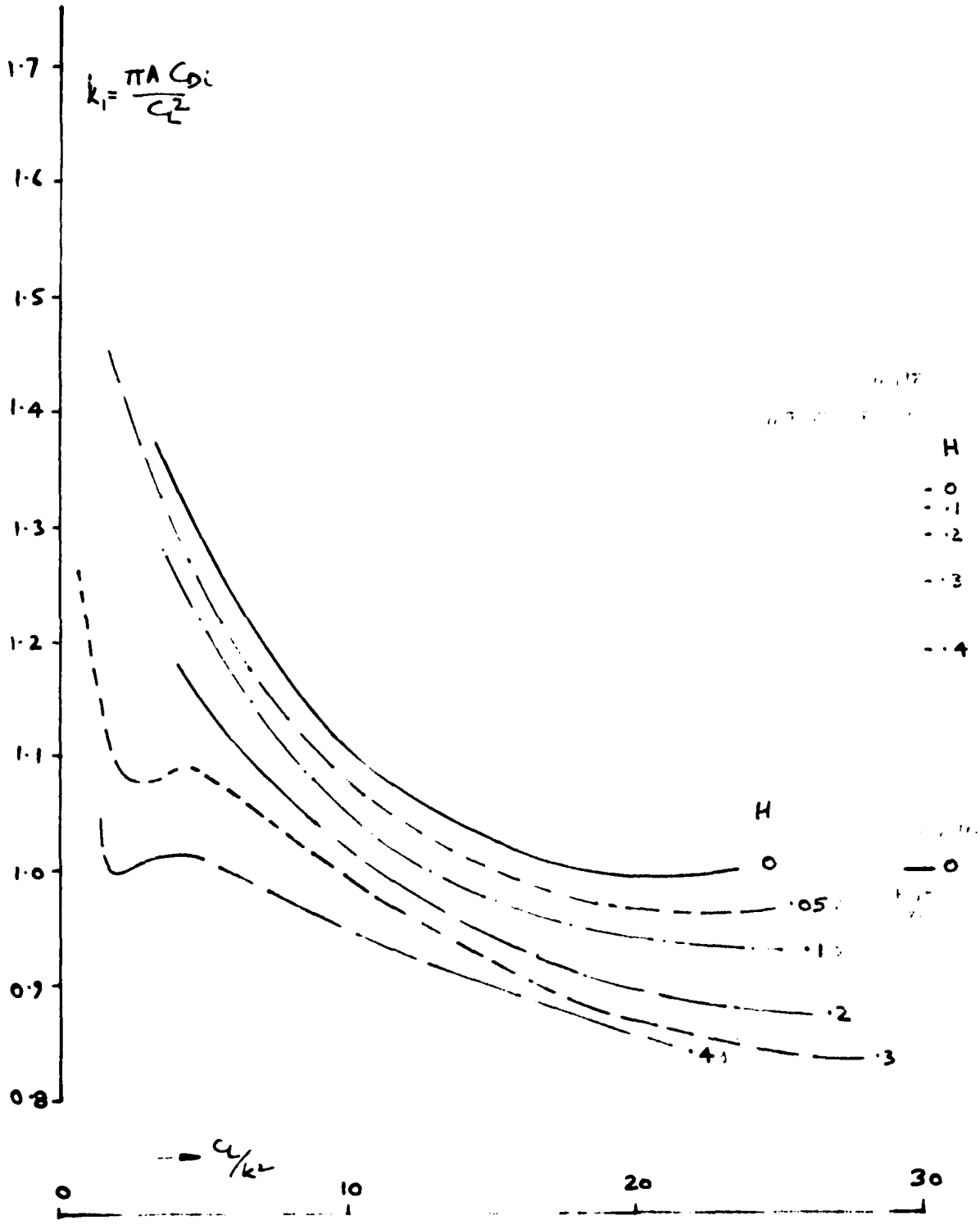

FIG. 21. CIRCULAR-ARC CAMBER WINGS
k_1 variation

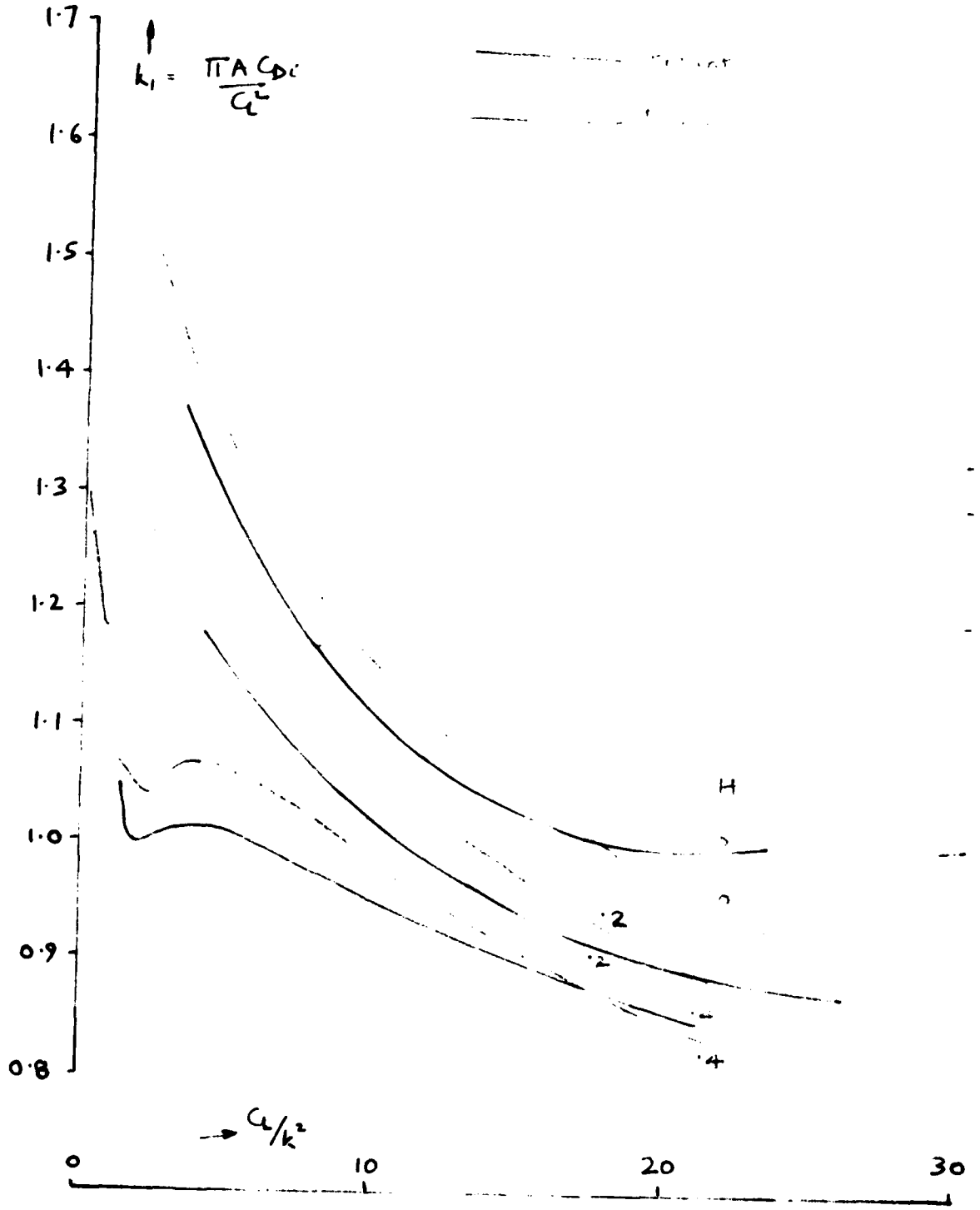

FIG. 22. CIRCULAR-ARC CAMBER WINGS
k_1 VARIATION - COMPARISON WITH BARSBY

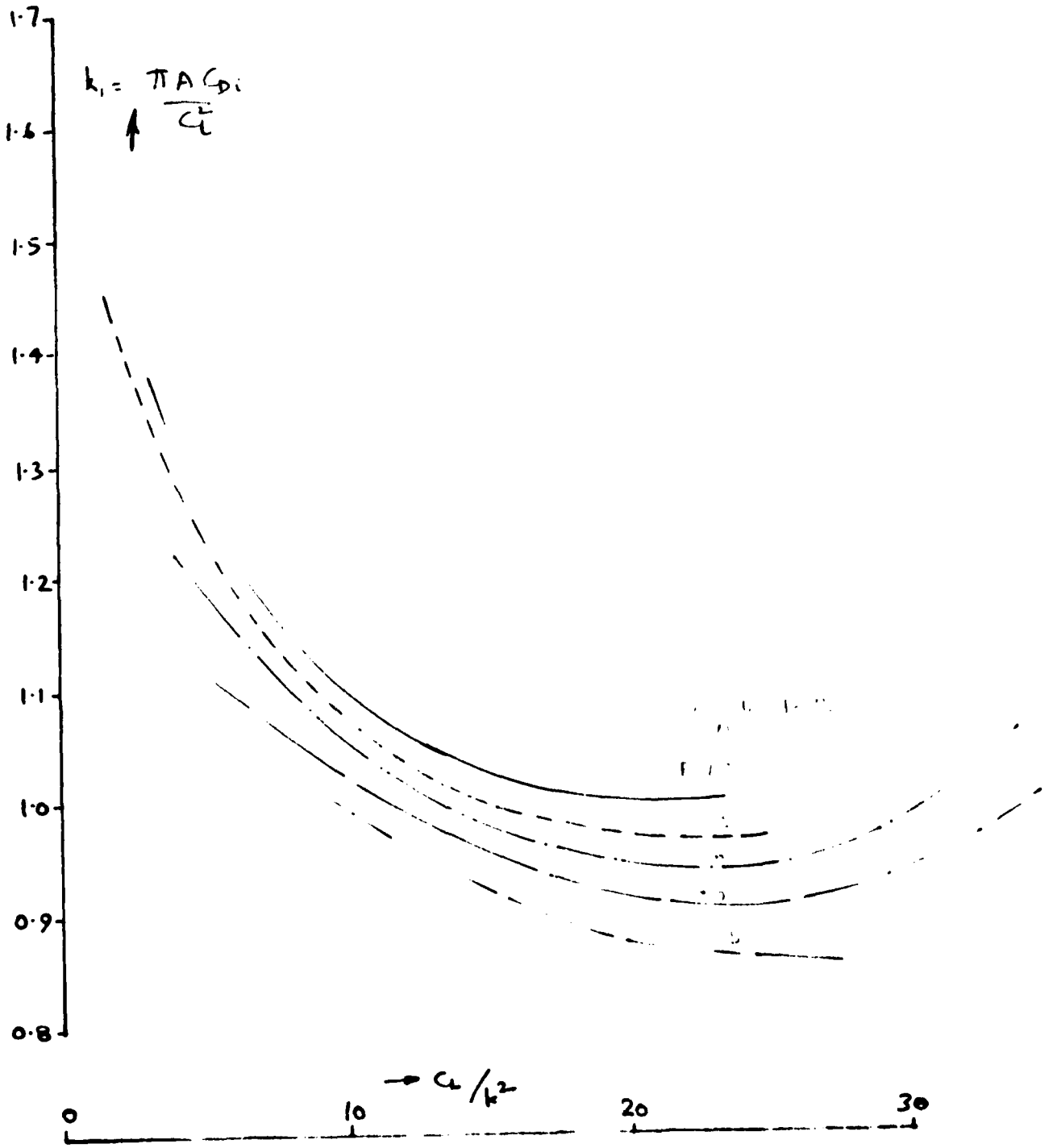

FIG. 23 WINGS WITH L.E. DROOP H = 0·05 S
k_1 VARIATION

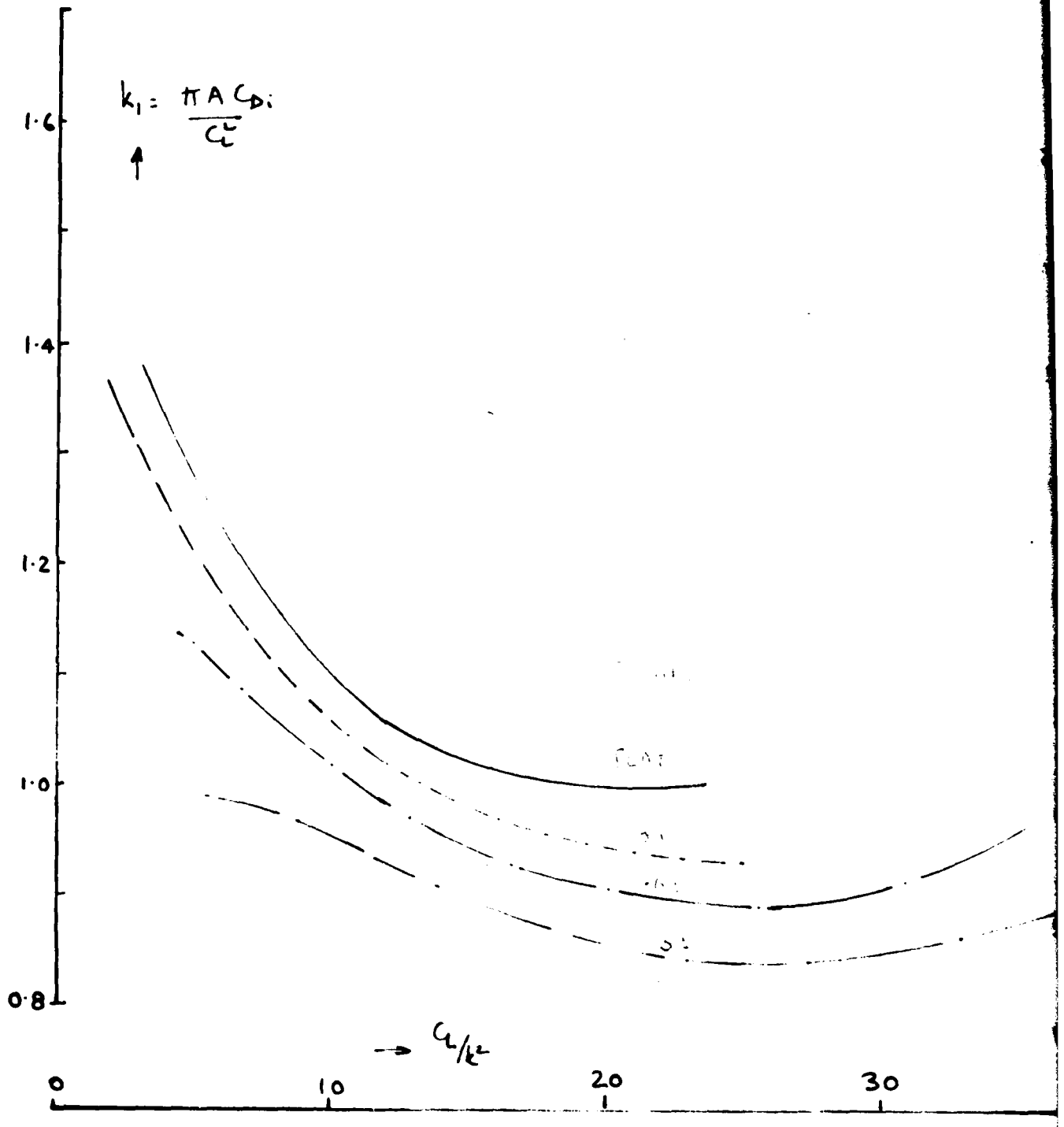

FIG. 24. WINGS WITH L.E. DROOP $H = 0.1\,s$
k_1 VARIATION

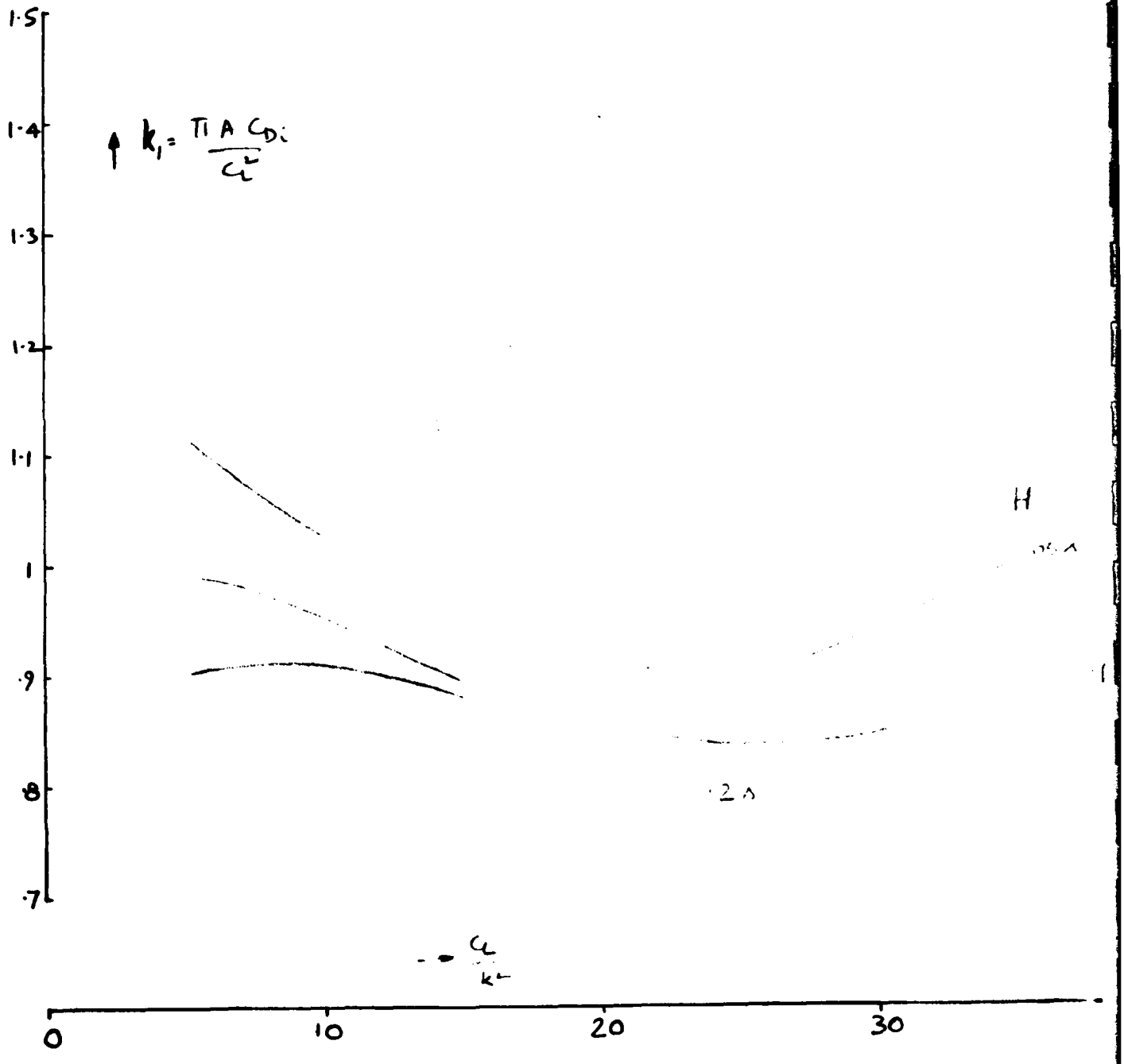

FIG. 25. WINGS WITH L.E. DROOP SHOULDER AT M = 0·6 ;
k_1 VARIATION

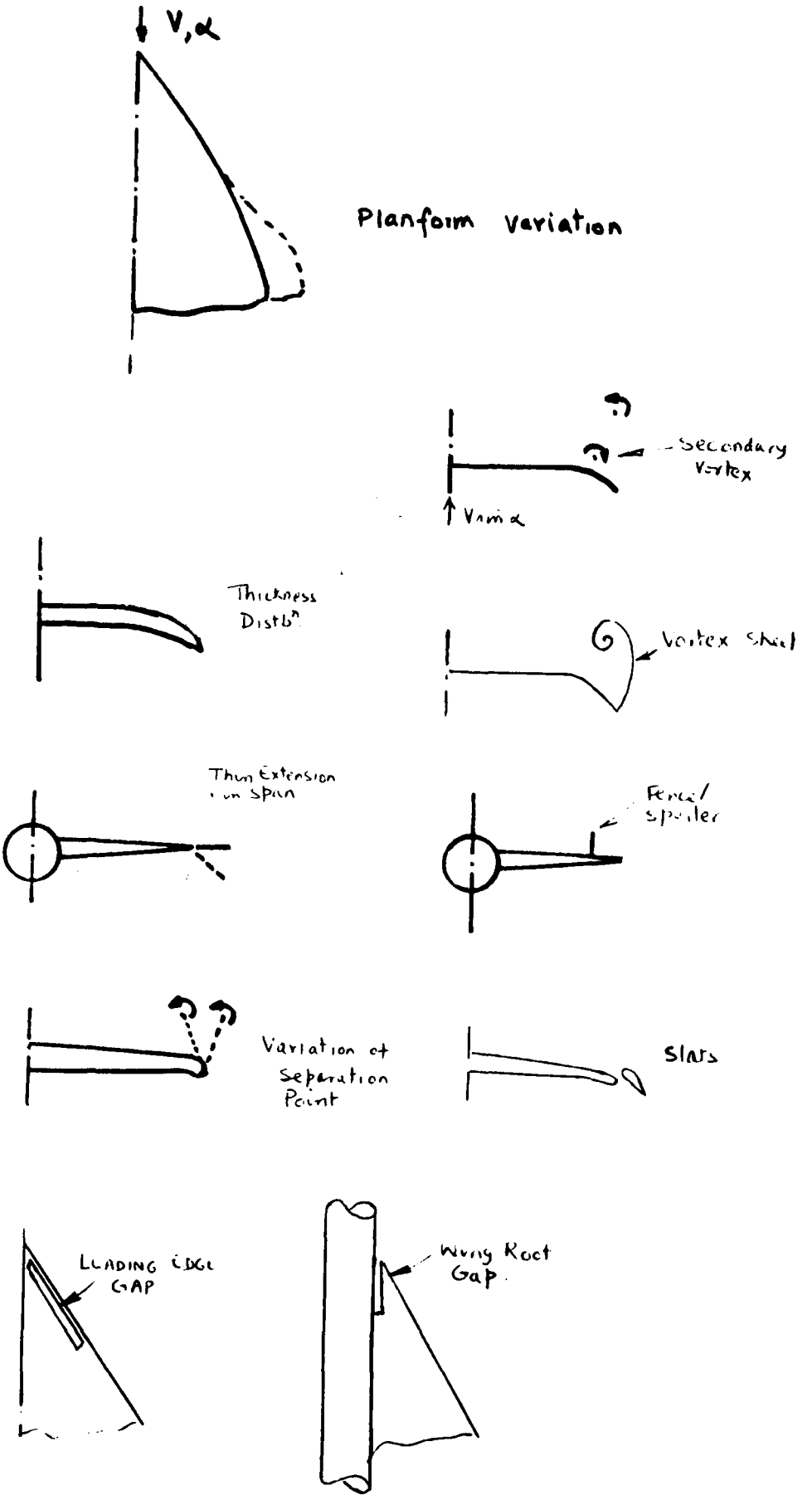
V, α
Planform Variation
Secondary Vortex
V sin α
Thickness Distb^n
Vortex Shed
Thin Extension on Span
Fence / Spoiler
Variation of Separation Point
Slats
LEADING EDGE GAP
Wing Root Gap

FIG. 26